A high resolution scheme for Eulerian gas-solid two-phase isentropic flow

Hudson, Justin and Harris, David

2006

MIMS EPrint: **2007.147**

Manchester Institute for Mathematical Sciences
School of Mathematics

The University of Manchester

Reports available from: http://eprints.maths.manchester.ac.uk/
And by contacting: The MIMS Secretary
School of Mathematics
The University of Manchester
Manchester, M13 9PL, UK

ISSN 1749-9097

Available online at www.sciencedirect.com
SCIENCE DIRECT®
Journal of Computational Physics 216 (2006) 494–525
JOURNAL OF COMPUTATIONAL PHYSICS
www.elsevier.com/locate/jcp

A high resolution scheme for Eulerian gas–solid two-phase isentropic flow

Justin Hudson *, David Harris

School of Mathematics, University of Manchester, Sackville Street, Manchester, M60 1QD, United Kingdom

Received 27 January 2005; received in revised form 16 December 2005; accepted 20 December 2005
Available online 7 February 2006

Abstract

Numerical solutions of the equations governing two-phase isentropic flow of a solid granular material dispersed in a gas are investigated. Both the dispersed and continuous phases are treated as continua and an Eulerian description of the flow is adopted. We present an inviscid model with a general pressure term from which a number of variant models can be obtained. A high resolution scheme is presented to obtain numerical approximations of the equations in each of the models. We investigate whether the chosen numerical scheme is suitable for the equations governing the models and use the numerical results to obtain quantitative and qualitative insight into the predictions of each of the models. Three test cases, new to the literature, are considered, and the numerical results compared.

AMS: 65M06; 76T25; 35l65

Keywords: Eulerian two-phase flow; Gas–solid; High resolution scheme; Inhomogeneous conservation laws

1. Introduction

Many industrial and engineering processes involve the flow of several intermingled phases (solid, liquid and gaseous) and/or chemical species. In particular, chemical engineers have been much involved with the development of models of multi-phase flow and their application. For example, flow in hoppers and risers, the separation and mixing of chemicals, various processes that occur in nuclear reactors and coal combustion are just a few of the areas where chemical engineering research into multi-phase systems plays an important role in industry. For many industrial applications, it is crucial to both model the process realistically and to obtain accurate approximations to the solutions of initial and boundary value problems arising from the process and the model, in order that the process runs efficiently, that costs are reduced and that plant and process are able to operate safely. The special case of two-phase flow is the most well developed theoretically and has numerous practical applications that are crucial to industry and which

* Corresponding author. Tel.: +44 0161 306 3217.
E-mail addresses: justin.hudson@manchester.ac.uk, juh@onetel.com (J. Hudson), david.harris@manchester.ac.uk (D. Harris).

0021-9991/$ - see front matter
doi:10.1016/j.jcp.2005.12.010

may involve any combination such as liquid–gas, gas–gas, etc. There is extensive literature devoted to two-phase flow in the context of problems arising in chemical engineering and Gidaspow [13] provides an excellent introduction to the subject.

In this paper we are concerned with one particular combination, namely a gas–solid two phase system in which the solid phase is a granular material (by which is meant that the solid phase material is finely subdivided into small separate grains in such a way that the volume of each grain is small in comparison to the total volume of solid) which has been dispersed in a gaseous phase. We shall refer to the gas as the continuous phase, the solid as the dispersed phase. Once dispersed the system will only remain so, at least in a terrestrial environment, if energy is continually input into the system to maintain the dispersion. This is effectively done by ensuring that the gas always *flows* and then momentum is consequently transferred from the gaseous to the solids phase by their mechanical interaction. A typical application is the pneumatic conveying of bulk solids, see Klinzing et al. [24].

There are three different approaches that are commonly made to modelling the flow of granular materials. Discrete methods [22] (for example, using particle or rigid body dynamics), statistical mechanics [28] (which generalises the theory of dense gases to include the inelastic collisions between grains) and continuum mechanics [21] (where both solid and fluid mechanics are applicable to granular materials, depending upon the deformation or flow regime). For the gas–solid systems of the type considered here, where the solids phase is dispersed in a flowing gas, the methods of fluid mechanics are appropriate with the solids phase being effectively modelled as a type of fluid. A hallmark of multi-phase flow is the use of hybrid models that utilise two or more of the above approaches. For example, the gas phase is modelled as a continuum, whereas the solids phase may be modelled in a discrete (Lagrangian) or continuum (Eulerian) way. The discrete Lagrangian method (see Huber and Sommerfeld [17]) models, and keeps track of, each particle individually, whilst the Eulerian method (see Gidaspow [13]) treats averaged bulk properties of the solids phase in terms of an equivalent fluid flow. In either case, the system of equations are sufficiently complicated to prevent analytical solutions being found in all but the most trivial cases and recourse must be had to numerical methods to obtain approximations of the equations. Due to the complexity of the models, this also is a non-trivial task and the solution of problems of relevance to industry required the advent of adequate computing power. As computing power increases, approximations to more and more complex problems of interest to industry will become feasible. The present paper is intended as a contribution towards this process by analysing methods of numerical approximation in the context of models which, on the one hand are sufficiently simple to enable progress to be made on their numerical analysis and on the other hand form a sufficiently adequate basis for this type of two-phase flow.

We take an Eulerian formulation of two-phase gas–solid flow in which both phases are treated as a continuum. The basic balance equations governing such models, together with appropriate constitutive equations, have been in a state of development since the 1960's, see Jackson [19], Rudinger and Chang [34], Gidaspow [13] and Jackson [20,21] for further information.

The range of applications of two-phase flow is extremely wide and encompasses many different physical processes. It is not possible for a single mathematical model to apply to all the diverse variety of two phase systems. For example the mechanics of bubbles in a liquid is very different from that of wind blown sand. The pneumatic conveying of glass beads at room temperature is very different from problems of combustion and detonation of reactive powders. We shall adopt a mathematical model appropriate to applications such as the pneumatic conveying of granular material at moderate pressures and at room temperature in cases of moderate gas velocity.

A careful distinction must be made between isentropic and non-isentropic flow. For applications at room temperature, moderate pressures and in the absence of significant shear layers an isentropic model is, as considered in this paper, applicable. Such models may be used when entropy production may be neglected or when its effects are considered unimportant for the calculated physical quantities. However, there are examples where isentropic models should not be used, an example here being combustion and deflagration of reactive granular materials. There is an extensive literature on such models, for both modelling and numerical aspects. We do not give a detailed description here, but following on from the work of Baer and Nunziato [1] we may cite Saurel and Abgrall [35], Bdzil et al. [2], Saurel and Lemetayer [36] and Powers [31]. Such models are intended for rather different purposes than the applications considered here, but

there is overlap in the methods used and in the modelling and numerical problems addressed. For example, the evolution equations governing the solids volume fraction is considered rate-dependent in combustion problems, while at room temperature and moderate pressures it may be modelled using rate-independent plasticity models, see for example Harris and Grekova [14]. Such issues merit further investigation.

In short, the essence of good modelling is to choose a model appropriate to the problem at hand, that is to say, as simple as possible while retaining sufficient physics and mechanics to approximate well enough the real system. It is also important to be aware of its limitations and to use it only in situations for which it is intended. The proper context here is the flow of granular materials in which the gas phase is the mechanism whereby momentum is transferred to the solids phase to enable the transportation of the solids phase. Mechanical energy is also transferred from the gas phase to the solids phase in the form of solids phase fluctuation energy.

In the early 1980s, Jenkins and co-workers extended the Kinetic Theory of dense gases to include granular materials by taking into account the energy loss during collisions, see, for example, Jenkins and Savage [23], Savage and Jeffrey [37] and Lun et al. [28]. The application of this theory in the chemical engineering context has been affected by its inclusion in models of gas–solid two-phase flow. One advantage of using the kinetic theory is that it enables certain material properties associated with the dispersed phase which are difficult to measure experimentally, for example the solids phase viscosity, to be calculated from the theory. Use of the kinetic theory of granular flow, however, introduces a new mechanical quantity together with an energy equation containing it. This quantity is called either the fluctuation energy or the granular temperature. The latter name is somewhat confusing and inappropriate and it must be understood that although the name granular temperature is used in analogy with the usual word temperature, it is a mechanical quantity and not a thermodynamic quantity and is nothing to do with heat content of the solids phase. A major purpose of the present paper is to investigate numerically the fluctuation energy equation.

Another major purpose is to develop a high resolution scheme [15] applicable to isentropic flows of solids/gas two phase models which contain the fluctuation energy equation, particular care being taken over the inhomogeneous terms in the equations, as these may present difficulties in implementation with high resolution schemes. The model is expressed in terms of a general pressure gradient, from which a number of different models may be obtained as special cases. Numerical solutions are obtained by implementing a high resolution scheme.

In the following section, we present and briefly discuss the equations governing the model containing a general pressure term used for two-phase gas–solid flow and introduce three special cases of this model. We investigate the hyperbolicity of the different models in Section 3. The model is discretised in Section 4 using a high resolution scheme discussed by Hubbard and Garcia-Navarro [16] and Hudson [18], based on Roe's scheme [32]. The models are then compared in Section 5 for a variety of test cases. Our conclusions are presented in Section 6.

2. Mathematical formulation

The numerical scheme is developed by considering a time varying flow in one space dimension of a two-phase gas–solid mixture. The typical application is pipe flow, with lateral dimension small in comparison to the length. The grain size is assumed to be reasonably small in comparison with the lateral dimension. The continuous gas phase and the dispersed solids phase are represented by separate interpenetrating continua at each point of space occupied by the mixture. In the real system each point in space is occupied solely by either gas or solid, but in the model, each point x possesses the attributes of both solid and fluid material. The underlying idea is that the phases are averaged over a representative volume element (RVE) large enough to contain both gas and grains, although the continuum model is phenomenological and no attempt is made to define or calculate the spatial averages explicitly. However, the introduction of the fluctuation energy T_s into the model ultimately uses the ensemble average of statistical mechanics, see Lun et al. [28], and so the model presented is a hybrid of continuum and statistical approaches.

The pipe lies along a portion OP of the real axis and a coordinate system Ox taken, with the origin O coinciding with the left hand end of the pipe, and positive x-direction pointing towards P. Let u_g, u_s denote the

Eulerian velocity components (in the x-direction) of the gas and solid phases, respectively, ρ_g, ρ_s the density of the gas and grains, defined at each point x of OP. In the real mixture, let V denote the volume of the RVE containing a representative mixture of gas and grain, V_g and V_s denote the volumes occupied by gas and grains, respectively. The gas and solid volume fractions ϵ_s and ϵ_g are defined by

$$\epsilon_g = \frac{V_g}{V} \quad \text{and} \quad \epsilon_s = \frac{V_s}{V}, \tag{1}$$

respectively, which satisfy the following properties

$$0 \leqslant \epsilon_g \leqslant 1, \quad 0 \leqslant \epsilon_s \leqslant 1 \quad \text{and} \quad \epsilon_g + \epsilon_s = 1. \tag{2}$$

Finally, let T_s denote the fluctuation energy or granular temperature of the solids phase. The physical interpretation of T_s is that it is the square of the deviation of the individual grain velocity from the mean grain velocity.

2.1. The model equations

The conservation laws governing the model are presented as follows, see for example Jackson [20,21]. Conservation of mass for each phase gives rise to the following continuity equations:

$$\frac{\partial}{\partial t}(\epsilon_g \rho_g) + \frac{\partial}{\partial x}(\epsilon_g \rho_g u_g) = 0, \tag{3a}$$

$$\frac{\partial}{\partial t}(\epsilon_s \rho_s) + \frac{\partial}{\partial x}(\epsilon_s \rho_s u_s) = 0. \tag{3b}$$

The momentum equations for the gas and solid phase are:

$$\frac{\partial}{\partial t}(\epsilon_g \rho_g u_g) + \frac{\partial}{\partial x}(\epsilon_g \rho_g u_g^2) + \omega_1 \frac{\partial p_g}{\partial x} + \omega_2 \frac{\partial p_s}{\partial x} = -\beta(u_g - u_s), \tag{3c}$$

$$\frac{\partial}{\partial t}(\epsilon_s \rho_s u_s) + \frac{\partial}{\partial x}(\epsilon_s \rho_s u_s^2) + \omega_3 \frac{\partial p_g}{\partial x} + \omega_4 \frac{\partial p_s}{\partial x} = \beta(u_g - u_s), \tag{3d}$$

respectively. Models vary in the way p_g and p_s are incorporated and the device of including the multipliers ω_k is to enable variations of the basic model to be conveniently written as a single set of equations. Various choices for ω_k are given in the following section.

We now discuss the above equations in detail. The mechanical interaction between the two phases is through the drag force, $\beta(u_g - u_s)$, present in both momentum equations.

Two commonly used forms for the drag force are (a) Stokes' law, for laminar flow and moderate relative velocities and which is linear in the phase velocity difference $u_g - u_s$, (b) Newton's law, for turbulent flow and which is quadratic in $u_g - u_s$. The latter is physically more appropriate in the case here where the dispersed phase consists of a large number of grains and in which the interaction between the phases significantly affects the gas flow. We take the coefficient β to be

$$\beta = \frac{3C_D}{4d_s}\epsilon_g \epsilon_s \rho_g |u_g - u_s|,$$

where C_D is a dimensionless parameter, which for the regime corresponding to Newton takes an approximate value of $C_D = 0.44$. For further discussion in the context of chemical engineering, see Gidaspow [11] and Klinzing et al. [24]. Thus, gas viscosity is taken into account via the gas on grain interaction.

For the applications we have in mind, for example, pneumatic conveying at moderate pressures and speed at room temperature, it is appropriate to assume the gas flow to be isentropic. We note that in the test cases described in Section 5, the numerical scheme allows for the proper evolution of the gas pressure field. In all three cases, the gas pressure is almost constant. The absence of large pressure gradients helps to confirm the validity of the isentropic assumption. We shall also assume that, in the gas flow (i.e., the gas on gas interaction), the effect of viscosity may be neglected. The gas phase is assumed to behave as an inviscid, compressible fluid obeying the perfect gas law. Let p_g^0 and ρ_g^0 denote standard pressure and the density at standard temperature and pressure and define

$$C_{\mathrm{p}} = \frac{p_{\mathrm{g}}^0}{(\rho_{\mathrm{g}}^0)^{\gamma_{\mathrm{g}}}},$$

then the gas pressure p_{g} satisfies

$$p_{\mathrm{g}}(\rho_{\mathrm{g}}) = C_{\mathrm{p}}\rho_{\mathrm{g}}^{\gamma_{\mathrm{g}}},$$

where C_{p} has dimensional properties $\mathrm{m}^{3\gamma_{\mathrm{g}}-1}/(\mathrm{kg}^{\gamma_{\mathrm{g}}-1}\,\mathrm{s}^2)$, i.e., viscosity is omitted from the gas constitutive equation and the stress tensor is diagonal. The solids pressure p_{s} is assumed to satisfy the following law, analogous to the perfect gas law for gases (and so solids phase viscosity is also omitted),

$$p_{\mathrm{s}}(\epsilon_{\mathrm{s}}, T_{\mathrm{s}}) = \epsilon_{\mathrm{s}}\rho_{\mathrm{s}}T_{\mathrm{s}}d_0, \quad \text{where } d_0 = 1 + 2(1 + r_{\mathrm{s}})g_0\epsilon_{\mathrm{s}},$$

where r_{s} is the coefficient of restitution and the radial distribution function [13] is

$$g_0(\epsilon_{\mathrm{s}}) = \frac{3}{5}\left[1 - \left(\frac{\epsilon_{\mathrm{s}}}{\epsilon_{\mathrm{s,max}}}\right)^{\frac{1}{3}}\right]^{-1},$$

where $\epsilon_{\mathrm{s,max}}$ denotes the maximum value of ϵ_{s} and reflects the fact that the most densely packed configuration of grains is approximately equal to 0.7. In practice the model becomes physically invalid at some value of ϵ_{s} less than 0.7, but the model is used for values of ϵ_{s} up to approximately 0.5. Finally T_{s} denotes the granular temperature or fluctuation energy of the solids phase.

As stated above, the typical application for these equations is to the pneumatic conveying of solids, where airborne solids at moderate gas velocities are transported by pipe. This regime is referred to in the literature on granular materials as fast flow. The solids phase is in suspension and grains interact by way of instantaneous binary collisions, caused by the fluctuation of the individual grain velocity from that of the mean grain velocity. This idea, taken from statistical mechanics, gives rise to the quantity T_{s} and forms the basis for the final solids equation, the fluctuation energy equation [6,41,4],

$$\frac{\partial}{\partial t}(\epsilon_{\mathrm{s}}\rho_{\mathrm{s}}T_{\mathrm{s}}) + \frac{\partial}{\partial x}(\epsilon_{\mathrm{s}}\rho_{\mathrm{s}}u_{\mathrm{s}}T_{\mathrm{s}}) = -\frac{2}{3}\left(p_{\mathrm{s}}\frac{\partial u_{\mathrm{s}}}{\partial x} + \gamma - \frac{\partial\left(\kappa\frac{\partial T_{\mathrm{s}}}{\partial x}\right)}{\partial x} + 3\beta T_{\mathrm{s}}\right). \tag{3e}$$

The first term on the RHS of this equation is responsible for the generation of fluctuation energy T_{s}, $p_{\mathrm{s}}(u_{\mathrm{s}})_x$, the second term causes its dissipation. The Jenkins and Savage [23] formula for dissipation of T_{s} is

$$\gamma = 3(1 - r_{\mathrm{s}}^2)\epsilon_{\mathrm{s}}^2\rho_{\mathrm{s}}g_0T_{\mathrm{s}}\left(\frac{4}{d_{\mathrm{s}}}\sqrt{\frac{T_{\mathrm{s}}}{\pi}} - (u_{\mathrm{s}})_x\right),$$

which is derived for slightly inelastic particles (i.e., r_{s} is close to 1). We follow the approach of [4,28,41] and neglect the $(u_{\mathrm{s}})_x$ term. The third term governs the diffusion of T_{s}, where κ is the diffusion coefficient and we use the formula of Gidaspow et al. [12],

$$\kappa = \frac{75}{192}\frac{\rho_{\mathrm{s}}d_{\mathrm{s}}\sqrt{\pi T_{\mathrm{s}}}}{(1 + r_{\mathrm{s}})g_0}\left(1 + \frac{6}{5}(1 + r_{\mathrm{s}})g_0\epsilon_{\mathrm{s}}\right)^2.$$

The final term, $-3\beta T_{\mathrm{s}}$, simulates the transfer of energy from the gas phase to the solids phase in the form of fluctuation energy, Ding and Gidaspow [6]. For a more detailed discussion of these terms, see Boemer et al. [4].

An algebraic formula was derived by Syamlal et al. [41] on the assumption of a balance between generation and dissipation of fluctuation energy, i.e.,

$$p_{\mathrm{s}}(u_{\mathrm{s}})_x + \gamma = 0.$$

However, we consider the full system including the time-dependent fluctuation energy equation.

The solids density ρ_{s} is assumed constant. This is both an accurate approximation and the simplest way to close the models. The gas density ρ_{g} is not assumed to be constant. The governing equations for the model are summarised in Table 1, where a subscript $k = \mathrm{g}$ ($k = \mathrm{s}$) denotes the gas phase (solids phase). Also, the physical quantities appearing in the model are summarised in Table 2.

Table 1
Summary of equations for the model

Conservation of mass,

$$(\epsilon_k\rho_k)_t + (\epsilon_k\rho_k u_k)_x = 0$$

Conservation of momentum (gas phase),

$$(\epsilon_g\rho_g u_g)_t + (\epsilon_g\rho_g u_g^2)_x + \omega_1(p_g)_x + \omega_2(p_s)_x = -\beta(u_g - u_s)$$

Conservation of momentum (solids phase),

$$(\epsilon_s\rho_s u_s)_t + (\epsilon_s\rho_s u_s^2)_x + \omega_3(p_g)_x + \omega_4(p_s)_x = \beta(u_g - u_s)$$

Fluctuation energy equation,

$$(\epsilon_s\rho_s T_s)_t + (\epsilon_s\rho_s u_s T_s)_x = -\frac{2}{3}(p_s(u_s)_x + \gamma - (\kappa(T_s)_x)_x + 3\beta T_s)$$

Gas pressure,

$$p_g(\rho_g) = C_p\rho_g^{\gamma_g}$$

Solids pressure,

$$p_s(\epsilon_s, T_s) = \epsilon_s\rho_s T_s d_0 \text{ with } d_0 = 1 + 2(1 + r_s)g_0\epsilon_s$$

Radial distribution function [13],

$$g_0(\epsilon_s) = \frac{3}{5}\left[1 - \left(\frac{\epsilon_s}{\epsilon_{s,max}}\right)^{\frac{1}{3}}\right]^{-1}$$

Drag force (Newton),

$$\beta = \frac{3C_D}{4d_s}\epsilon_g\epsilon_s\rho_g|u_g - u_s| \quad \text{where } C_D = 0.44$$

Dissipation of fluctuation energy [23],

$$\gamma = \frac{12}{d_s}(1 - r_s^2)\epsilon_s^2\rho_s g_0 T_s\sqrt{\frac{T_s}{\pi}}$$

Diffusion of fluctuating energy [12],

$$\kappa = \frac{75}{192}\frac{\rho_s d_s\sqrt{\pi T_s}}{(1 + r_s)g_0}(1 + \frac{6}{5}(1 + r_s)g_0\epsilon_s)^2$$

Sum of volume fractions,

$$\epsilon_g + \epsilon_s = 1$$

Table 2
Physical quantities in the model

Name	Symbol	Units
Density	$\rho_k(x,t)$	kg/m^3
Velocity	$u_k(x,t)$	m/s
Granular temperature	$T_s(x,t)$	m^2/s^2
Volume fraction	$\epsilon_k(x,t)$	None
Gravity	g	m/s^2
Gas pressure	$p_g(\rho_g)$	kg/(m s^2)
Solids pressure	$p_s(\epsilon_s, T_s)$	kg/(m s^2)
Drag force	β	kg/(m^3 s)
Solids particle diameter	d_s	m
Coefficient of restitution	r_s	None
Gas viscosity	μ_g	Pa s
Maximum solids volume fraction	$\epsilon_{s,max}$	None

2.2. Gas and solids data

We consider the case of glass beads being transported by air and take a solids density of $\rho_s = 2660\ \mathrm{kg/m^3}$ and particle diameter $d_s = 0.005$ m. For the gas phase, data corresponding to air at room temperature (20 °C) with atmospheric pressure (100.0437 kPa), density $\rho_g = 1.2885\ \mathrm{kg/m^3}$ and viscosity $\mu_g = 1.58 \times 10^{-7}$ Pa s are taken. Also, $\gamma_g = 1.4$ and $C_p = 75{,}916.16\ \mathrm{m^{3.2}/(kg^{0.4}\ s^2)}$. The coefficient of restitution (unless otherwise stated) is $r_s = 0.99$ (typically, the value of r_s is taken to be close to 1, see Jenkins and Savage [23]). If collisions are elastic (i.e., no loss of fluctuating energy) then $r_s = 1$, which results in $\gamma = 0$. The maximum value of the solids volume fraction is taken as $\epsilon_{s,\max} = 0.7$.

Since the gas flow is at moderate velocities and room temperature it is physically appropriate to assume an isentropic gas flow. Thus, shocks in the gas phase are not permissible. However, two-phase flows have a richer shock structure than single-phase and there are shocks involving the solids phase which, for the gas phase only involve discontinuities in ϵ_g and u_g, while ρ_g remains continuous. Such shocks do not violate the assumption of constant entropy. Perturbations in the gas phase evolve on a considerably faster time scale than those of the solids phase, since $|\lambda_g| \gg |\lambda_s|$, so shocks due to the solids phase propagate slowly in comparison with the gas speed of sound.

2.3. Different models

A number of special cases may be obtained from the model given in the previous section by choosing appropriate values of the multipliers ω_k, thus determining which pressure terms are present. Adding the two-phase momentum equations must give the balance of momentum for the mixture as a whole and so there are restrictions on the values of the ω_k, to ensure that the mixture equation has the correct total pressure term, in fact, $\omega_1 + \omega_3$ and $\omega_2 + \omega_4$ must be equal to either zero or one. Two models are as follows.

2.3.1. Model A

Much fundamental work on two-phase flow has been done by Jackson, see for example, Jackson [19], one of the first papers to derive the classic two-phase flow equations and obtained by setting

$$\omega_1 = \epsilon_g, \quad \omega_2 = 0, \quad \omega_3 = \epsilon_s \quad \text{and} \quad \omega_4 = 0.$$

This is often known as the equal pressure model and is the foundation for much work on two-phase flow. With the advent of a kinetic theory of granular flow, the fluctuation energy equation and solids pressure were incorporated into Jackson's model, see Ding and Gidaspow [6], Boemer et al. [4] and Bouillard et al. [5], giving the following model, termed Model A

$$\omega_1 = \epsilon_g, \quad \omega_2 = 0, \quad \omega_3 = \epsilon_s \quad \text{and} \quad \omega_4 = 1.$$

2.3.2. Model B

Rudinger and Chang [34] develop an alternative model to that of Jackson [19], and which is extended by Lyczkowski [29], by having the gas pressure present only in the gas phase, i.e.,

$$\omega_1 = 1, \quad \omega_2 = 0, \quad \omega_3 = 0 \quad \text{and} \quad \omega_4 = 0.$$

This model is an inviscid version of the "dusty gas" equations, see Foster et al. [9]. As with Model A, the fluctuation energy equation and solids pressure have been incorporated into the model, see Bouillard et al. [5], Boemer et al. [4] and Gidaspow [13]. Model B, is obtained by taking

$$\omega_1 = 1, \quad \omega_2 = 0, \quad \omega_3 = 0 \quad \text{and} \quad \omega_4 = 1.$$

2.3.3. Model C

A third possibility is to place the pressure terms symmetrically in the momentum equations, and we refer to this as Model C

$$\omega_1 = \omega_2 = \epsilon_g \quad \text{and} \quad \omega_3 = \omega_4 = \epsilon_s.$$

For this model, the gas and solids pressure appear in the momentum equations for both phases.

3. Hyperbolicity

In this section we consider whether each model is hyperbolic for the regime under investigation, both for the suitability of the scheme and for the implementation of the initial and boundary conditions for the test cases. We solve the equations only in regimes where the equations are hyperbolic and need to investigate when this is the case.

In the case where the system of partial differential equations considered here possess all real wave speeds (obtained from the canonical form) a full set of linearly independent eigenvectors exists and so the model is hyperbolic, see LeVeque [26]. Rewriting the system of equations for the model with the general pressure term (3) in canonical form

$$\begin{bmatrix} \rho_g \\ u_g \\ \epsilon_s \\ u_s \\ T_s \end{bmatrix}_t + \begin{bmatrix} u_g & \rho_g & \frac{\rho_g}{\epsilon_g}(u_s - u_g) & \frac{\rho_g \epsilon_s}{\epsilon_g} & 0 \\ \frac{\omega_1 c_g^2}{\epsilon_g \rho_g} & u_g & \frac{\omega_2 c_s^2}{\epsilon_g \rho_g} & 0 & \frac{\omega_2 \epsilon_s \rho_s d_0}{\epsilon_g \rho_g} \\ 0 & 0 & u_s & \epsilon_s & 0 \\ \frac{\omega_3 c_g^2}{\rho_s \epsilon_s} & 0 & \frac{\omega_4 c_s^2}{\rho_s \epsilon_s} & u_s & \omega_4 d_0 \\ 0 & 0 & 0 & \frac{2}{3} T_s d_0 & u_s \end{bmatrix} \begin{bmatrix} \rho_g \\ u_g \\ \epsilon_s \\ u_s \\ T_s \end{bmatrix}_x = \begin{bmatrix} 0 \\ -\frac{\beta}{\epsilon_g \rho_g}(u_g - u_s) \\ 0 \\ \frac{\beta}{\rho_s \epsilon_s}(u_g - u_s) \\ -\frac{2}{3\rho_s \epsilon_s}(\gamma + 3\beta T_s) \end{bmatrix},$$

where

$$c_g^2 = \frac{\partial p_g}{\partial \rho_g} = C_p \gamma_g \rho_g^{\gamma_g - 1}, \quad c_s^2 = \frac{\partial p_s}{\partial \epsilon_s} = \rho_s T_s (d_0 + \epsilon_s c_0^2) \quad \text{and} \quad c_0^2 = \frac{\partial d_0}{\partial \epsilon_s}.$$

The diffusion term in the fluctuation energy equation has a negligible effect on T_s, for the values of κ and T_s given by Eq. (3e). Thus, we neglect this term from the fluctuation energy equation.

For this system, the characteristic equation is

$$(\lambda - u_s) Q(\lambda) = 0,$$

where $Q(\lambda)$ is the quartic,

$$Q(\lambda) = a_4 \lambda^4 + a_3 \lambda^3 + a_2 \lambda^2 + a_1 \lambda + a_0,$$

whose components are:

$$\begin{aligned}
a_4 &= 3\rho_s \epsilon_g, \quad a_3 = -6\rho_s \epsilon_g (u_g + u_s), \\
a_2 &= -3c_g^2(\omega_1 \rho_s + \omega_3 \rho_g) - \omega_4 \rho_s \epsilon_g T_s (3d_0 + 2d_0^2 + 3\epsilon_s c_0^2) + 3\rho_s \epsilon_g (u_s^2 + u_g^2 + 4u_g u_s), \\
a_1 &= 6c_g^2(\omega_1 \rho_s u_s + \omega_3 \rho_g u_g) + 2\omega_4 \rho_s \epsilon_g u_g T_s (3\epsilon_s c_0^2 + 3d_0 + 2d_0^2) - 6\rho_s \epsilon_g u_g u_s (u_s + u_g), \\
a_0 &= -3c_g^2(\omega_1 \rho_s u_s^2 + \omega_3 \rho_g u_g^2) + 3\rho_s \epsilon_g u_g^2 u_s^2 + \rho_s T_s ((\omega_1 \omega_4 - \omega_3 \omega_2) c_g^2 - \omega_4 \epsilon_g u_g^2)(2d_0^2 + 3d_0 + 3\epsilon_s c_0^2).
\end{aligned}$$

Thus, one root is always real and the other four are determined by solving the quartic. The roots of the quartic for the model in general have not been found analytically. Thus, we investigate each of the three special cases individually. If analytic expressions for the roots are not available we use Matlab to investigate the quartic numerically. We use the constant values in Section 2.2 and then solve the quartic for a variety of values of the remaining variables appearing in the coefficients a_k. The Matlab program calculates the values of a_k, calculates the roots numerically using the built in command $c = \text{roots}(a_k)$ and determines if any root is complex by using the command image(c), with image(c) $\neq 0$ if a root is complex.

3.1. Model A

Analytical expressions of the wave strengths for Model A are difficult to obtain thus, we use Matlab to determine the roots numerically. Figs. 1 and 2 illustrate various contour plots for certain fixed values of ϵ_s, ρ_g and T_s to show combinations of values resulting in complex roots. The coefficients of the quartic may readily be rewritten in terms of $u_g - u_s$ and $u_g + u_s$ and from Fig. 1, we can see that $u_g - u_s$ plays an important role. The graph shows two regions of real roots, both dependent on $u_g - u_s$. The region of real roots for small relative velocities (R1) increases in width as T_s is increased whereas the real region of real roots for large relative velocities (R2) is slightly reduced. Moreover, as ϵ_s is increased, the region R1 increases in width whereas the region R2 is reduced in width. Changing the gas density also has an impact on the region of real roots and reduces the width of both regions R1 and R2. This behaviour is verified by Fig. 2. Thus, Model A is hyperbolic for a restricted set of values of the quantities appearing in the coefficients.

The results show that fixed values of $u_g - u_s = C$, where C is a constant, produces identical regions of real roots, regardless of the individual values of u_g and u_s. Setting one velocity equal to zero simplifies the analysis and Fig. 3 illustrates the graph of the quartic for different relative velocities with one of the velocities equal to zero. From the results, we can see that the real region R1 is created by a maximum, which appears at $\lambda \approx u_s$, and is destroyed when the value of the quartic is less than zero for the position of this maximum, i.e., $Q(u_s) < 0$. By letting $u_s = 0$, we see the maximum remains approximately at the origin for

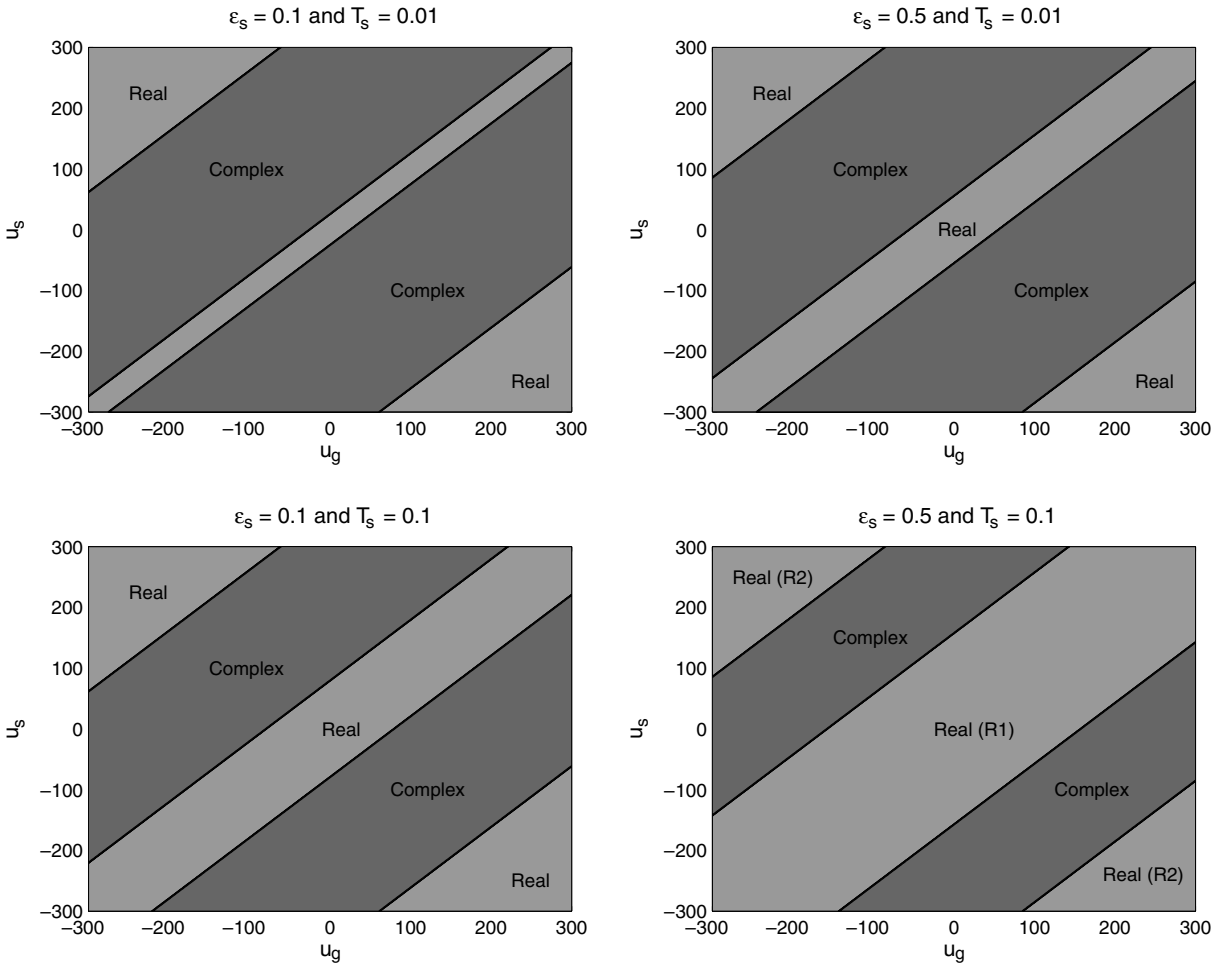

Fig. 1. Hyperbolicity of Model A for different velocities.

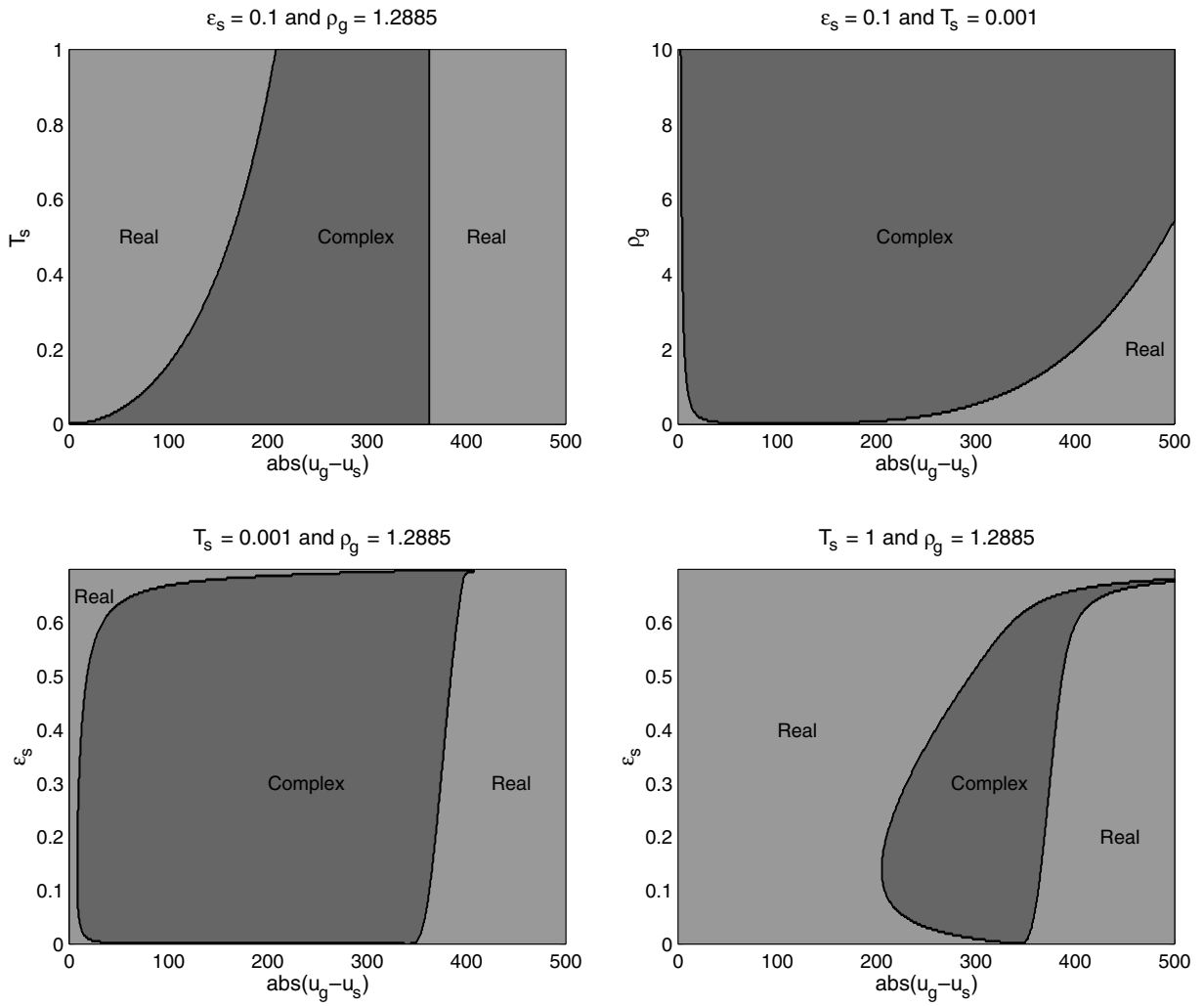

Fig. 2. Hyperbolicity of Model A for $u_g = 0$.

small relative velocities. Thus, by assuming the position of the maximum is at $\lambda = u_s$ and by letting $u_s = 0$, we obtain the following inequality:

$$-3c_g^2\epsilon_s\rho_g u_g^2 + \rho_s T_s \epsilon_g (c_g^2 - u_g^2)(2d_0^2 + 3d_0 + 3\epsilon_s c_0^2) > 0,$$

which determines whether or not the region of real roots R1 exists. A similar inequality in terms of u_s can be obtained by setting $u_g = 0$. Thus, since the region of real roots is unaltered for the same relative velocities, we obtain a more general inequality

$$(u_g - u_s)^2 < \frac{\rho_s T_s \epsilon_g c_g^2 (2d_0^2 + 3d_0 + 3\epsilon_s c_0^2)}{3c_g^2\epsilon_s\rho_g + \rho_s T_s \epsilon_g (2d_0^2 + 3d_0 + 3\epsilon_s c_0^2)}$$

to determine the maximum value of relative velocities allowed for the real region R1. When compared to the position of the maximum computed by Matlab using $Q(\lambda) = 0$, in every run performed the inequality gave a good indication of the true value, and, in every case, correctly predicted the existence of real roots.

In conclusion, for Model A there exists a small region of real roots when the relative velocity is sufficiently small. It is known that the original model of Jackson [19] for inviscid flow, i.e., $p_s = 0$, is not hyperbolic for small relative velocities, see Lyczkowski et al. [30], Drew [7] and Stewart and Wendroff [38]. However, by including the solids pressure term in the solids phase, a new region of real roots for small relative velocities

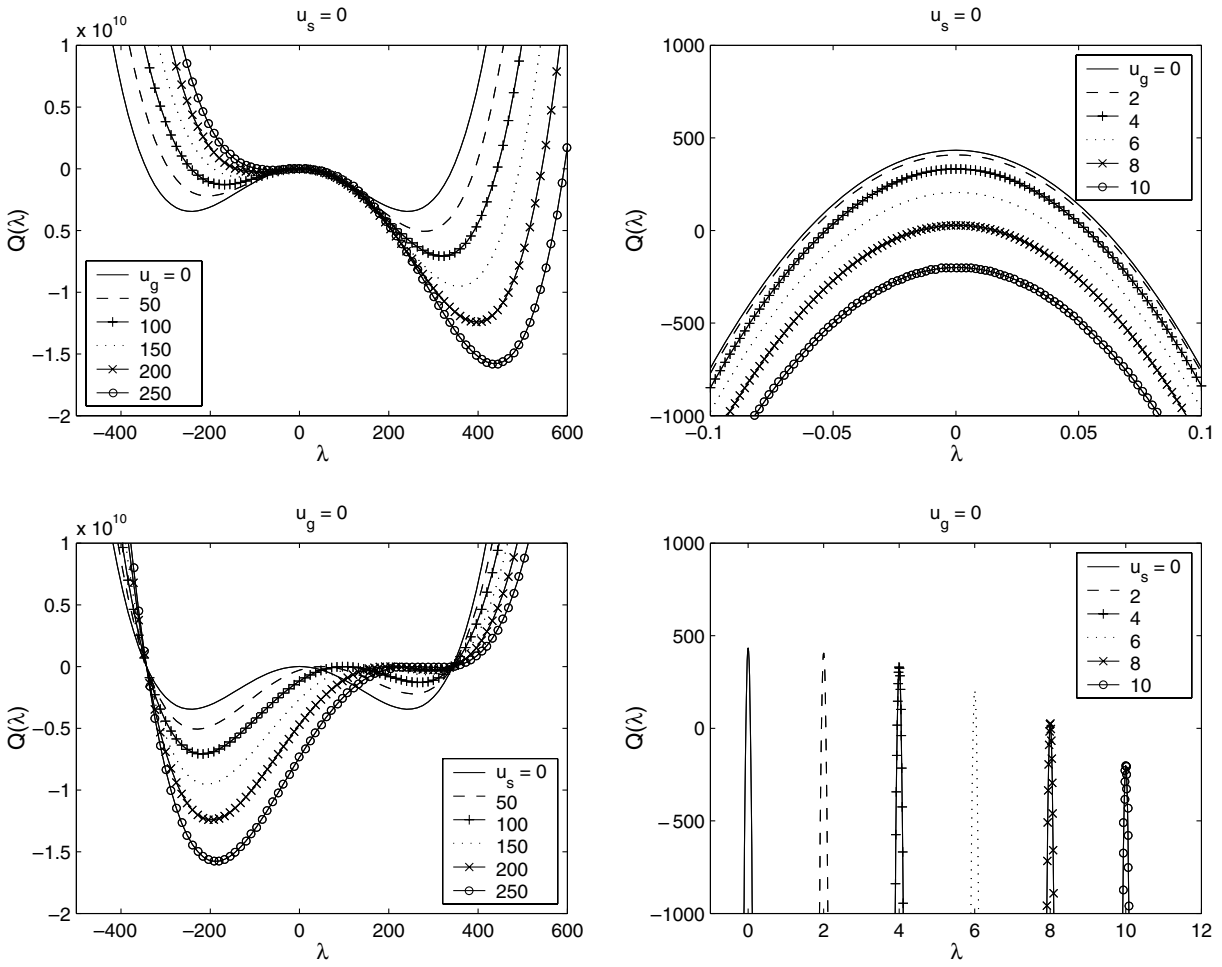

Fig. 3. Analysis of the quartic for Model A with $T_s = 0.001$, $\rho_g = 1.2885$ and $\epsilon_s = 0.1$.

is created. Moreover, for the model presented here, $p_s = 0$ only if either $\epsilon_s = 0$ or $T_s = 0$. If there is a region of pure gas, i.e., $\epsilon_s = 0$, the quartic has four real roots. When $T_s = 0$, two of the roots of the quartic are complex for small relative velocities, but the model is not valid in this limit, since then there are no velocity fluctuations and hence no collisions between grains.

3.2. Model B

For Model B, the roots of the quartic are determined analytically,

$$\lambda_{1,2} = u_g \pm c_g\sqrt{\epsilon_g^{-1}}, \quad \lambda_3 = u_s \quad \text{and} \quad \lambda_{4,5} = u_s \pm \frac{1}{3}\sqrt{T_s(9d_0 + 9\epsilon_s c_0^2 + 6d_0^2)}.$$

Hence, Model B is hyperbolic since there are 5 real and distinct eigenvalues. Moreover, two of the roots are associated with the gas-phase ($\lambda_{1,2}$) and three with the solids-phase ($\lambda_{3,4,5}$).

3.3. Model C

As with Model A, analytical expressions of the wave strengths for Model A are difficult to obtain thus, we use Matlab. Figs. 4 and 5 illustrate the same numerical tests carried out with Model A. Model C has real roots for $u_g = u_s$ and is hyperbolic for y large values of $u_g - u_s$. However, the small interval of real roots for small relative velocities, which is present in Model A, is no longer present.

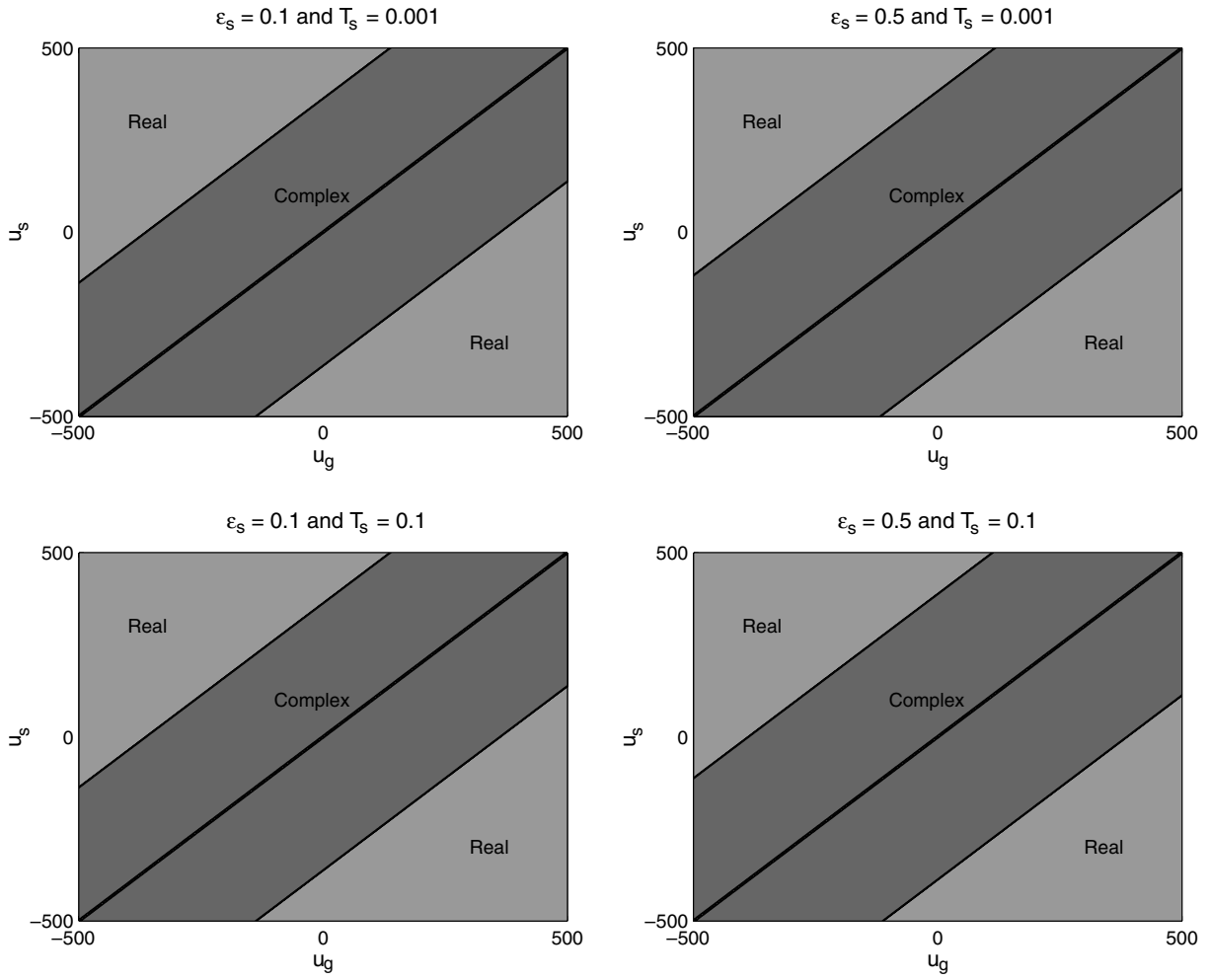

Fig. 4. Hyperbolicity of Model C for different velocities.

Thus, by including the solids pressure in both the gas and solids phase, i.e., $\omega_2 = \omega_4 = \epsilon_g$, the small interval of real roots (R1) created by the solids pressure in the solids phase is destroyed. Models A and C are both hyperbolic for large relative velocity, but Model C is not hyperbolic (having two complex roots) for small relative velocities. Henceforth we no longer consider Model C.

4. Numerical discretisation

In this section, we discretise the model with the general pressure term and discuss a high resolution scheme that can be used to obtain numerical approximations to the solutions of the model for regimes in which the equations are hyperbolic.

4.1. Model formulation

The model with the general pressure terms, Section 2, may be written in the form

$$\mathbf{w}_t + \mathbf{F}(\mathbf{w})_x = \mathbf{R} + \mathbf{S}, \tag{4}$$

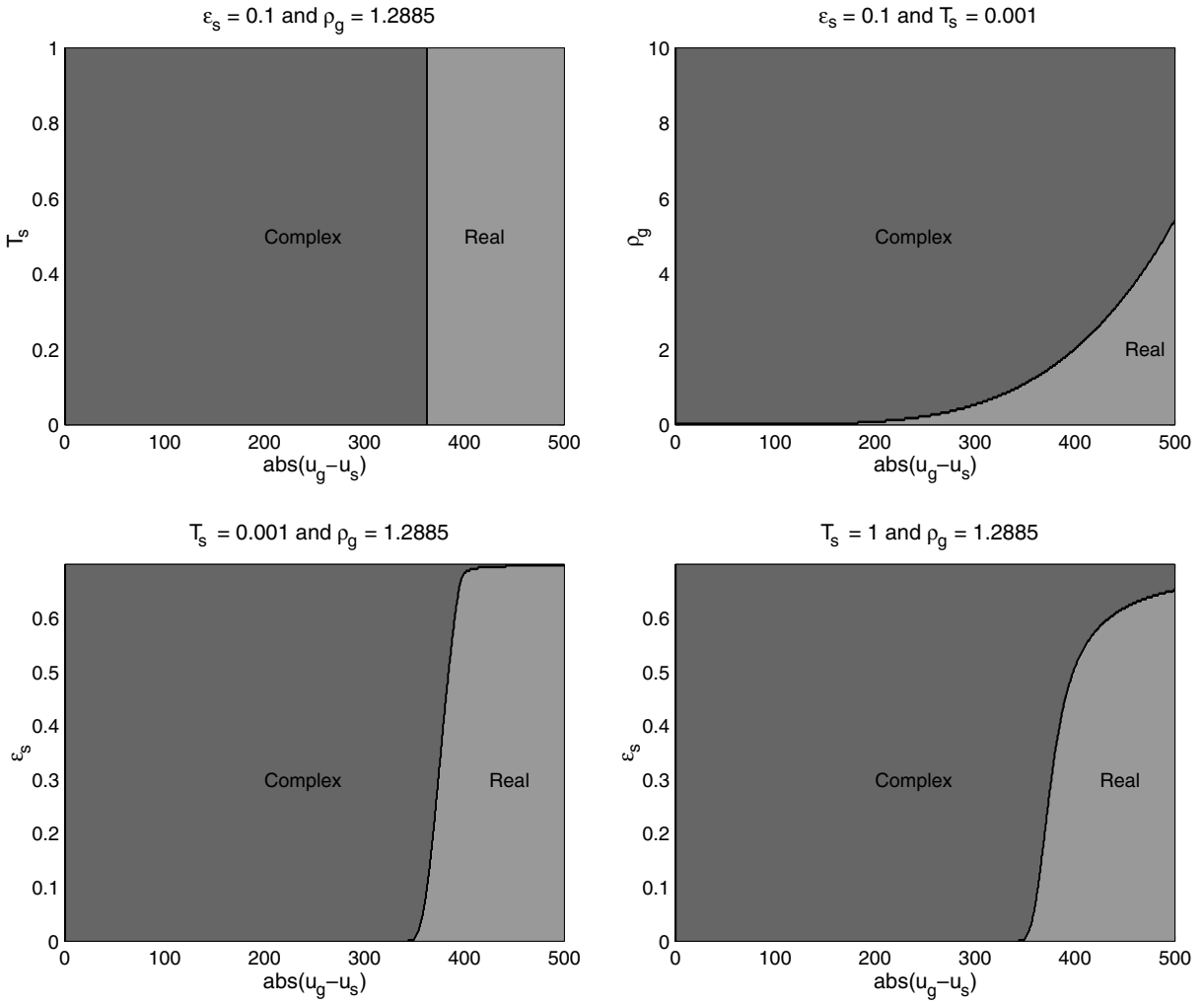

Fig. 5. Hyperbolicity of Model C for $u_g = 0$.

where

$$\mathbf{w} = \begin{bmatrix} \epsilon_g \rho_g \\ \epsilon_g \rho_g u_g \\ \epsilon_s \\ \epsilon_s u_s \\ \epsilon_s T_s \end{bmatrix}, \quad \mathbf{R} = \begin{bmatrix} 0 \\ (1-\omega_1)(p_g)_x - \omega_2 \rho_s (\epsilon_s T_s d_0)_x \\ 0 \\ -\frac{\omega_3}{\rho_s}(p_g)_x + (1-\omega_4)(\epsilon_s T_s d_0)_x \\ -\frac{2}{3}\epsilon_s T_s d_0 (u_s)_x \end{bmatrix}, \quad \mathbf{F}(\mathbf{w}) = \begin{bmatrix} \epsilon_g \rho_g u_g \\ \epsilon_g \rho_g u_g^2 + p_g \\ \epsilon_s u_s \\ \epsilon_s u_s^2 + \epsilon_s T_s d_0 \\ \epsilon_s u_s T_s \end{bmatrix} \quad \text{and}$$

$$\mathbf{S} = \begin{bmatrix} 0 \\ -\beta(u_g - u_s) \\ 0 \\ \frac{\beta}{\rho_s}(u_g - u_s) \\ -\frac{2}{3\rho_s}(3\beta T_s - (\kappa(T_s)_x)_x + \gamma) \end{bmatrix}.$$

Here, $\mathbf{F}(\mathbf{w})$ denotes the flux-function. The inhomogeneous terms are split into those containing first order spatial derivatives of the dependent variables, $\mathbf{R}$, and those that do not, $\mathbf{S}$. We discretise the general model in the form (4) in order to enable shocks to form in the solids phase, for otherwise, discretising the model in quasi-linear form (or in a form not in terms of the original conserved variables), shocks may propagate

at incorrect speeds or the model may converge to a weak solution inconsistent with the equations of the original model. Since the gas flow is assumed to be isentropic, the model must only be used in regimes where there are no shocks involving the pressure and density in the gas phase. In two phase flow, discontinuities are allowed in the gas velocity and gas volume fraction, but such discontinuities are not thermodynamic in nature and hence do not violate the condition of constant entropy.

The equations for two phase systems differ from that of a single phase in the sense that for a single phase system the pressure gradient term is in conservation form, whereas for a two phase system it is not. We now extract the conserved part of the pressure gradient and include it in the homogeneous part in order for the two phase system to correspond more closely to the two single phase systems. The effect of this transformation is to render the physical waves speeds of the conserved two phase system analogous to those of the single phase systems. Thus, in the above formulation, the momentum equations (3c) and (3d) include part of the pressure gradient terms in the flux function, using

$$\omega_1(p_g)_x = (p_g)_x + (\omega_1 - 1)(p_g)_x \quad \text{and} \quad \omega_4(p_s)_x = (p_s)_x + (\omega_4 - 1)(p_s)_x.$$

The system obtained in this way is such that the homogeneous part has a Jacobian with distinct real eigenvalues and is hence hyperbolic. The wave speeds of this system also correspond closely to the wave speeds of the system written in canonical form. The Jacobian matrix of the system is

$$\mathbf{J} = \begin{bmatrix} 0 & 1 & 0 & 0 & 0 \\ \epsilon_g^{-1}c_g^2 - u_g^2 & 2u_g & \rho_g\epsilon_g^{-1}c_g^2 & 0 & 0 \\ 0 & 0 & 0 & 1 & 0 \\ 0 & 0 & \epsilon_s T_s c_0^2 - u_s^2 & 2u_s & d_0 \\ 0 & 0 & -u_s T_s & T_s & u_s \end{bmatrix}$$

with eigenvalues

$$\lambda_{1,2} = u_g \mp c_g\sqrt{\epsilon_g^{-1}}, \quad \lambda_3 = u_s, \quad \lambda_{4,5} = u_s \mp c_s,$$

where the speed of sound for pure gas is

$$c_g = \sqrt{\frac{\partial p_g}{\partial \rho_g}} = \sqrt{C_p\gamma_g\rho_g^{\gamma_g - 1}}$$

and the solids propagation velocity is

$$c_s = \sqrt{\frac{1}{\rho_s}\frac{\partial p_s}{\partial \epsilon_s}} = \sqrt{T_s(d_0 + \epsilon_s c_0^2)}$$

with

$$c_0^2 = \frac{\partial d_0}{\partial \epsilon_s} = 2(1 + r_s)\left(g_0 + \epsilon_s\frac{\partial g_0}{\partial \epsilon_s}\right)$$

and

$$\frac{\partial g_0}{\partial \epsilon_s} = \frac{1}{5(\epsilon_s^2\epsilon_{s,\max})^{\frac{1}{3}}}\left(1 - \left(\frac{\epsilon_s}{\epsilon_{s,\max}}\right)^{\frac{1}{3}}\right)^{-2}.$$

Having formulated the model in conservation form, we now investigate its numerical approximation.

4.2. High resolution scheme

We propose a numerical scheme to approximate the general system discussed in the previous section. The scheme is chosen to be second order accurate away from discontinuities and minimises the dispersion present

in second order schemes by adding dissipation in the neighbourhood of a discontinuity, i.e., we choose a high resolution scheme [15]. Since the system under investigation is inhomogeneous, the high resolution scheme must be capable of successfully incorporating the inhomogeneous terms. Inhomogeneous terms are renowned for creating numerical difficulties, see for example LeVeque and Yee [27], with numerous techniques being developed to try and resolve them, see Gascon and Corberan [10], LeVeque [25] and Bermúdez and Vázquez [3].

We use a high resolution scheme discussed by Hubbard and Garcia-Navarro [16], which is based on Roe's scheme [32]. We consider two different methods of approximating the inhomogeneous terms: a pointwise method and an upwind method. The upwind method applies flux-limiters, see Sweby [39], to the inhomogeneous terms as well as the flux-function to ensure a balance occurs between the terms for steady state problems (known as the *C*-property [3], see Appendix B). Both methods have been widely used for the shallow water equations and Euler's equations with varying degrees of success. We adapt the scheme for the Eulerian gas–solid two-phase flow models considered here. The scheme consists of

$$\mathbf{w}_i^{n+1} = \mathbf{w}_i^n - s(\mathbf{F}^*_{i+\frac{1}{2}} - \mathbf{F}^*_{i-\frac{1}{2}}) + s\mathbf{R}_i^* + \Delta t \mathbf{S}_i^n \tag{5}$$

with numerical flux-function

$$\mathbf{F}^*_{i+\frac{1}{2}} = \frac{1}{2}(\mathbf{F}^n_{i+1} + \mathbf{F}^n_i) - \frac{1}{2}\sum_{k=1}^{5}\left[\tilde{\alpha}_k|\tilde{\lambda}_k|(1 - \Phi(\tilde{\theta}_k)(1 - |\tilde{\nu}_k|))\tilde{\mathbf{e}}_k\right]_{i+\frac{1}{2}}.$$

The inhomogeneous terms not containing first order derivatives, $\mathbf{S}$, are approximated using a pointwise approach,

$$\mathbf{S}_i^n = \begin{bmatrix} 0 \\ -\beta(u_g - u_s) \\ 0 \\ \frac{\beta}{\rho_s}(u_g - u_s) \\ -\frac{2}{3\rho_s}\left(\gamma - \frac{\Delta(\kappa\Delta T_s)}{2\Delta x^2} + 3\beta T_s\right) \end{bmatrix}^n_i,$$

where

$$\Delta(\kappa\Delta T_s) = (\kappa^n_{i+1} + \kappa^n_i)(T_s)^n_{i+1} - (\kappa^n_{i+1} + 2\kappa^n_i + \kappa^n_{i-1})(T_s)^n_i + (\kappa^n_i + \kappa^n_{i-1})(T_s)^n_{i-1}$$

and the inhomogeneous terms containing first order derivatives, $\mathbf{R}$, are approximated by using one of the following.

1. A pointwise (PW) method, where the inhomogeneous terms are discretised at the mesh point and central differences are used when required,

$$\mathbf{R}_i^* = \begin{bmatrix} 0 \\ (1 - \omega_1)^n_i \Delta p_g - \rho_s(\omega_2)^n_i \Delta(\epsilon_s T_s d_0) \\ 0 \\ -\frac{(\omega_3)^n_i}{\rho_s}\Delta p_g + (1 - \omega_4)^n_i \Delta(\epsilon_s T_s d_0) \\ -\frac{2}{3}(\epsilon_s T_s d_0)^n_i \Delta u_s \end{bmatrix}, \tag{6}$$

   where $\Delta w = \frac{1}{2}(w^n_{i+1} - w^n_{i-1})$.
2. An upwind characteristic (CP) method,

$$\mathbf{R}_i^* = \mathbf{R}^-_{i+\frac{1}{2}} + \mathbf{R}^+_{i-\frac{1}{2}}, \tag{7}$$

where

$$\mathbf{R}^{\pm}_{i+\frac{1}{2}} = \frac{1}{2}\sum_{k=1}^{5}\left[\tilde{\beta}_k\tilde{\mathbf{e}}_k(1 \pm \mathrm{sgn}(\tilde{\lambda}_k)(1 - \Phi(\tilde{\theta}_k)(1 - |\tilde{\nu}_k|)))\right]_{i+\frac{1}{2}}.$$

The step sizes in space and time are Δx and Δt with i and n denoting the spatial and time grid number, respectively. The upstream and downstream boundaries are at x_0 and x_I (I is the total number of spatial grid points), t_N is the final time,

$$s = \frac{\Delta t}{\Delta x}, \quad \tilde{v}_k = s\tilde{\lambda}_k, \quad \tilde{\theta}_k = \frac{(\tilde{\alpha}_k)_{J+\frac{1}{2}}}{(\tilde{\alpha}_k)_{J+\frac{1}{2}}}, \quad J = i - \mathrm{sgn}(\tilde{v}_k)_{i+\frac{1}{2}},$$

and either the minmod flux-limiter [39],

$$\Phi(\theta) = \max(0, \min(1, \theta)), \tag{8}$$

or the van Leer [42] flux-limiter,

$$\Phi(\theta) = \frac{|\theta| + \theta}{1 + |\theta|}, \tag{9}$$

is used.To ensure the scheme remains stable, the time step is calculated using

$$\Delta t = \frac{v\Delta x}{\max(|\lambda|)},$$

where $\max(|\lambda|)$ is the maximum wave speed and $v \leqslant 1$ is the required Courant number.

The scheme is an adapted form of Roe's scheme [32], which uses piecewise constant data to represent the domain and can be viewed as a family of Riemann problems due to a small discontinuity being present between each neighbouring cell $(\mathbf{w}_\mathrm{R}, \mathbf{w}_\mathrm{L})$. This allows the system of homogeneous conservation laws,

$$\mathbf{w}_t + \mathbf{F}_x = 0$$

to be rewritten as a linearised Riemann problem,

$$\mathbf{w}_t + \tilde{\mathbf{A}}(\mathbf{w}_\mathrm{R}, \mathbf{w}_\mathrm{L})\mathbf{w}_x = 0,$$

where the Jacobian $\tilde{\mathbf{A}}$ is constant locally. The numerical solution of the resulting linear problem requires an appropriate Roe averaged (denoted by $\tilde{}$) Jacobian matrix, determined by solving

$$\Delta\mathbf{F} = \sum_{k=1}^{5} \tilde{\alpha}_k \tilde{\lambda}_k \tilde{\mathbf{e}}_k = \tilde{\mathbf{A}}\Delta\mathbf{w},$$

whilst ensuring that the u-properties of Roe are satisfied. The Roe averaged eigenvalues $(\tilde{\lambda})$ and eigenvectors $(\tilde{\mathbf{e}})$ are then calculated from the Roe averaged Jacobian. The decomposition

$$\Delta\mathbf{w} = \sum_{k=1}^{5} \tilde{\alpha}_k \tilde{\mathbf{e}}_k \quad \text{and} \quad \frac{1}{\Delta x}\sum_{k=1}^{5} \tilde{\beta}_k \tilde{\mathbf{e}}_k = \tilde{\mathbf{R}},$$

where $\Delta\mathbf{w} = \mathbf{w}_\mathrm{R} - \mathbf{w}_\mathrm{L}$, is then used to obtain the wave strengths $(\tilde{\alpha})$ and inhomogeneous values $(\tilde{\beta})$.

A full derivation of the Roe averages for the general system is presented in Appendix A and a summary is given in Table 3, where the superscripts denote the corresponding system. The high resolution scheme can now be used to approximate the general system of equations for various multipliers ω_k.

We are now in a position to obtain numerical solutions of the different models for a variety of test problems and to compare the results.

5. Numerical results

We now investigate the behaviour of the different models and the high resolution scheme for the gas–solid flow as discussed in Section 2.2. In order to compare the different models, we consider a variety of test cases all

Table 3
Roe average values for the general system

Roe averages,

$$\tilde{\rho}_g = \frac{\sqrt{(\epsilon_g)_L}(\rho_g)_L + \sqrt{(\epsilon_g)_R}(\rho_g)_R}{\sqrt{(\epsilon_g)_L} + \sqrt{(\epsilon_g)_R}}, \quad \tilde{u}_g = \frac{\sqrt{(\epsilon_g\rho_g)_L}(u_g)_L + \sqrt{(\epsilon_g\rho_g)_R}(u_g)_R}{\sqrt{(\epsilon_g\rho_g)_L} + \sqrt{(\epsilon_g\rho_g)_R}},$$

$$\tilde{c}_g = \begin{cases} \sqrt{\frac{\Delta p_g}{\Delta \rho_g}} & \text{if } \Delta\rho_g \neq 0, \\ c_g(\rho_g) & \text{otherwise,} \end{cases} \quad \tilde{c}_s^2 = \tilde{T}_s(\tilde{d}_0 + \tilde{\epsilon}_s\tilde{c}_0^2), \quad \tilde{d}_k = \frac{(\tilde{\lambda}_k - \tilde{u}_g)^2\tilde{\epsilon}_g - \tilde{c}_g^2}{\tilde{\rho}_g\tilde{c}_g^2}$$

$$\tilde{u}_s = \frac{\sqrt{(\epsilon_s)_L}(u_s)_L + \sqrt{(\epsilon_s)_R}(u_s)_R}{\sqrt{(\epsilon_s)_L} + \sqrt{(\epsilon_s)_R}}, \quad \tilde{T}_s = \frac{\sqrt{(\epsilon_s)_L}(T_s)_L + \sqrt{(\epsilon_s)_R}(T_s)_R}{\sqrt{(\epsilon_s)_L} + \sqrt{(\epsilon_s)_R}}, \quad \tilde{\epsilon}_k = \sqrt{(\epsilon_k)_R(\epsilon_k)_L},$$

$$\tilde{d}_0 = \frac{\sqrt{(\epsilon_s)_L}(d_0)_L + \sqrt{(\epsilon_s)_R}(d_0)_R}{\sqrt{(\epsilon_g)_L} + \sqrt{(\epsilon_g)_R}} \quad \text{and} \quad \tilde{c}_0 = \begin{cases} \sqrt{\frac{\Delta d_0}{\Delta \epsilon_s}} & \text{if } \Delta\epsilon_s \neq 0, \\ c_0(\epsilon_s) & \text{otherwise.} \end{cases}$$

Eigenvalues,

$$\tilde{\lambda}_{1,2} = \tilde{u}_g \mp \tilde{c}_g\sqrt{\tilde{\epsilon}_g^{-1}}, \tilde{\lambda}_3 = \tilde{u}_s \quad \text{and} \quad \tilde{\lambda}_{4,5} = \tilde{u}_s \mp \tilde{c}_s.$$

Eigenvectors,

$$\tilde{\mathbf{e}}_{1,2} = \begin{bmatrix} 1 \\ \tilde{\lambda}_{1,2} \\ 0 \\ 0 \\ 0 \end{bmatrix} \quad \text{and} \quad \tilde{\mathbf{e}}_k^{3,4,5} = \begin{bmatrix} 1 \\ \tilde{\lambda}_k \\ \tilde{d}_k \\ \tilde{\lambda}_k\tilde{d}_k \\ \frac{\tilde{d}_k}{\tilde{d}_0}((\tilde{\lambda}_k - \tilde{u}_s)^2 - \tilde{\epsilon}_s\tilde{T}_s\tilde{c}_0^2) \end{bmatrix}.$$

Wave strengths,

$$\tilde{\alpha}_{1,2} = \mp\frac{\tilde{\lambda}_3\tilde{\alpha}_3 + \tilde{\lambda}_4\tilde{\alpha}_4 + \tilde{\lambda}_5\tilde{\alpha}_5 - (\tilde{\alpha}_3 + \tilde{\alpha}_4 + \tilde{\alpha}_5 - \Delta(\epsilon_g\rho_g))\tilde{\lambda}_{2,1} - \Delta(\epsilon_g\rho_g u_g)}{\tilde{\lambda}_1 - \tilde{\lambda}_2},$$

$$\tilde{\alpha}_3 = -\frac{\tilde{d}_0\tilde{\epsilon}_s\Delta T_s}{\tilde{d}_3\tilde{c}_s^2} \quad \text{and} \quad \tilde{\alpha}_{4,5} = \frac{1}{2\tilde{d}_{4,5}\tilde{c}_s^2}(\Delta(\epsilon_s T_s d_0) \mp \tilde{c}_s\tilde{\epsilon}_s\Delta u_s).$$

Inhomogeneous terms,

$$\tilde{\beta}_k^{3,4,5} = \frac{(2\tilde{u}_s - \tilde{\lambda}_a - \tilde{\lambda}_b)\tilde{r}_4 + \tilde{d}_0\tilde{r}_5}{\tilde{d}_k(\tilde{\lambda}_k - \tilde{\lambda}_a)(\tilde{\lambda}_k - \tilde{\lambda}_b)} \quad \text{and} \quad \tilde{\beta}_{1,2} = \mp\frac{\tilde{\lambda}_3\tilde{\beta}_3 + \tilde{\lambda}_4\tilde{\beta}_4 + \tilde{\lambda}_5\tilde{\beta}_5 - (\tilde{\beta}_3 + \tilde{\beta}_4 + \tilde{\beta}_5)\tilde{\lambda}_{2,1} - \tilde{r}_2}{\tilde{\lambda}_1 - \tilde{\lambda}_2},$$

where $\tilde{r}_4 = -\frac{\omega_3}{\rho_s}\Delta p_g + (1 - \omega_4)\Delta(\epsilon_s T_s d_0)$,

$\tilde{r}_2 = (1 - \omega_1)\Delta p_g - \rho_s\omega_2\Delta(\epsilon_s T_s d_0)$ and $\tilde{r}_5 = -\frac{2}{3}\tilde{d}_0\tilde{\epsilon}_s\tilde{T}_s\Delta u_s$.

of which consist of a domain OP, 100 m long. Unless stated otherwise, the high resolution scheme is used with $\Delta x = 1$ m (i.e., 100 grid points) and a Courant number $v = 0.8$.

We only solve the general system when it is hyperbolic and require appropriate initial and boundary conditions for each test case. Unless otherwise stated, the numerical scheme uses free flow boundary conditions,

$$\mathbf{w}_{-i}^{n+1} = \mathbf{w}_0^n \quad \text{and} \quad \mathbf{w}_{I+i}^{n+1} = \mathbf{w}_I^n.$$

For the regime under investigation, the gas phase is subcritical whilst the solids phase may be supercritical. Thus, if physical boundary conditions are required only four can be prescribed at the upstream boundary and one at the downstream boundary.

5.1. Advection test problem

The first test case is a simple solids advection problem where an analytical solution can be obtained and is useful in determining that the numerical scheme is behaving appropriately. We obtain an analytical solution of the full model by assuming that the gas density and both phase velocities are constants,

$$\rho_g(x,t) = C_\rho \quad \text{and} \quad u_g(x,t) = u_s(x,t) = C_u.$$

Thus, the model simplifies to

$$(\epsilon_s)_t + C_u(\epsilon_s)_x = 0, \quad (p_s)_x = 0 \quad \text{and} \quad (T_s)_t + C_u(T_s)_x = -\frac{2}{3}(\gamma - (\kappa(T_s)_x)_x).$$

Assuming collisions are elastic, $r_s = 1$, so $\gamma = 0$, and by setting the diffusion coefficient $\kappa = 0$, we obtain the following analytical solution:

$$\epsilon_s(x,t) = \epsilon_s(x - C_u t, 0) \quad \text{and} \quad T_s(x,t) = \frac{C_T}{\epsilon_s d_0},$$

where C_T is a constant. To simulate a solids pulse propagating downstream, we use the initial conditions,

$$\epsilon_s(x,0) = \begin{cases} 0.1 + 0.1\sin^2\left(\frac{\pi}{10}(x-5)\right) & \text{if } 5 \leqslant x \leqslant 15, \\ 0.1 & \text{otherwise,} \end{cases}$$

with

$$C_\rho = 1.2885, \quad C_T = 0.001 \quad \text{and} \quad C_u = 5.$$

Table 4 denotes the L_1 error,

$$||\mathbf{E}||_1 = \Delta x \sum_{i=0}^{I} |\mathbf{E}_i^N|, \quad \text{where } \mathbf{E} = \mathbf{w}(x,t) - \mathbf{w}_i^n$$

for the sum of all variables at $t = 10$ s (N is the total number of time steps required to reach this time) for both first order ($\Phi = 0$) and high resolution (with minmod limiter) versions of the Scheme (5). The numerical solution converges to the analytical solution as the mesh size is reduced. Notice that the results of both models are almost identical with the first order results producing a higher L_1 error than the high resolution scheme. These findings are verified in Fig. 6, where it is clear that the first order scheme suffers more from diffusion. Thus, the results show that the high resolution scheme is superior to the first order version of the scheme.

5.2. Square pulse test problem

For the second test case, we simulate a square pulse of solids in the centre of the domain, which is at rest. In this simple simulation, we imagine that "walls" at $x = 40$ m and $x = 60$ m confine the solids to the region $40 < x < 60$ of the domain and they are kept in suspension by a "stirrer". The "walls" are then removed at time $t = 0$ and the solids are allowed to move freely. The initial conditions for this test case are

$$\rho_g(x,0) = 1.2885, \quad u_g(x,0) = u_s(x,0) = 0, \quad T_s(x,0) = 0.01\epsilon_s(x,0)$$

and

$$\epsilon_s(x,0) = \begin{cases} 0.2 & \text{if } 40 \leqslant x \leqslant 60, \\ 0.1 & \text{otherwise.} \end{cases}$$

Table 4
The L_1 error of the scheme at $t = 10$ s

Model	Scheme	$\Delta x = 1$	0.5	0.1	0.05	0.01
A	FO	0.97005	0.76820	0.32796	0.19609	0.04723
A	HR	0.56395	0.28067	0.02763	0.00790	0.00039
B	FO	0.97005	0.76820	0.32796	0.19609	0.04723
B	HR	0.56395	0.28067	0.02763	0.00790	0.00039

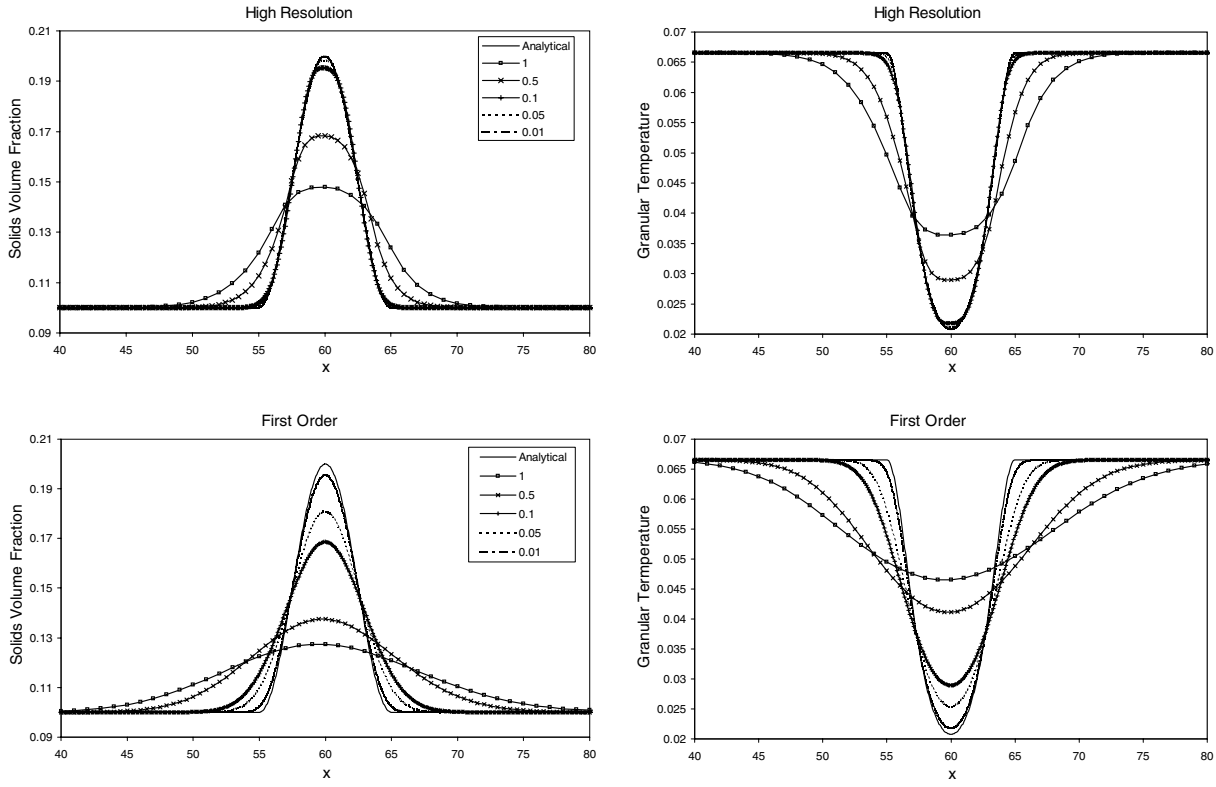

Fig. 6. Results of the advection test problem at $t = 10$ s.

The granular temperature (fluctuation energy) of the grains is higher within the region of the square pulse compared to that outside in order to simulate the effect of a stirrer.

For this test case, we assume that the collisions are elastic, i.e., the coefficient of restitution is $r_s = 1$.

Figs. 7 and 8 illustrate the results of the square pulse test problem at $t = 200$ s for the different models using the high resolution scheme (5) with the minmod limiter (8) and either the upwind (7) or pointwise (6) approximation for the inhomogeneous terms with first derivatives, respectively. Two spatial step sizes were used: the standard $\Delta x = 1$ m and a fine mesh (FM) of $\Delta x = 0.1$ m.

Models A and B produce practically identical results. The upwind method (CP) for the inhomogeneous terms produces a numerical kink at the stagnation point ($x = 50$ m), which is not present in the results for the pointwise method (PW). It occurs when the solids velocity changes sign and can be reduced by using a finer mesh. A similar problem arises in single-phase gas dynamics in cases where the entropy condition is violated, see LeVeque [26] for more information. However, the results show that the discretisation of the inhomogeneous terms is responsible because it is absent using the pointwise method. Moreover, it also occurs with the first order version of the scheme, $\Phi = 0$, thus applying limiters for the approximation of the inhomogeneous terms with first order derivatives is not the cause of the problem. Pointwise discretisation appears to be more accurate than the upwind method for this test case. See Sweby [40] for an example of a similar situation.

Fig. 9 illustrates the evolution of the test case for the fine mesh results, where the results are shown on a coarser grid (100 grid points) instead of the computed grid (1000 grid points). Initially the square pulse starts to collapse with two waves propagating in opposite directions. The shapes of the waves are such that after 40 s a peak has appeared at each side of the square pulse in the granular temperature. Although it appears to be similar to an entropy violation, the HLLE scheme [8] was used as a check and produced identical results to those displayed here, indicating that there is no entropy violation.

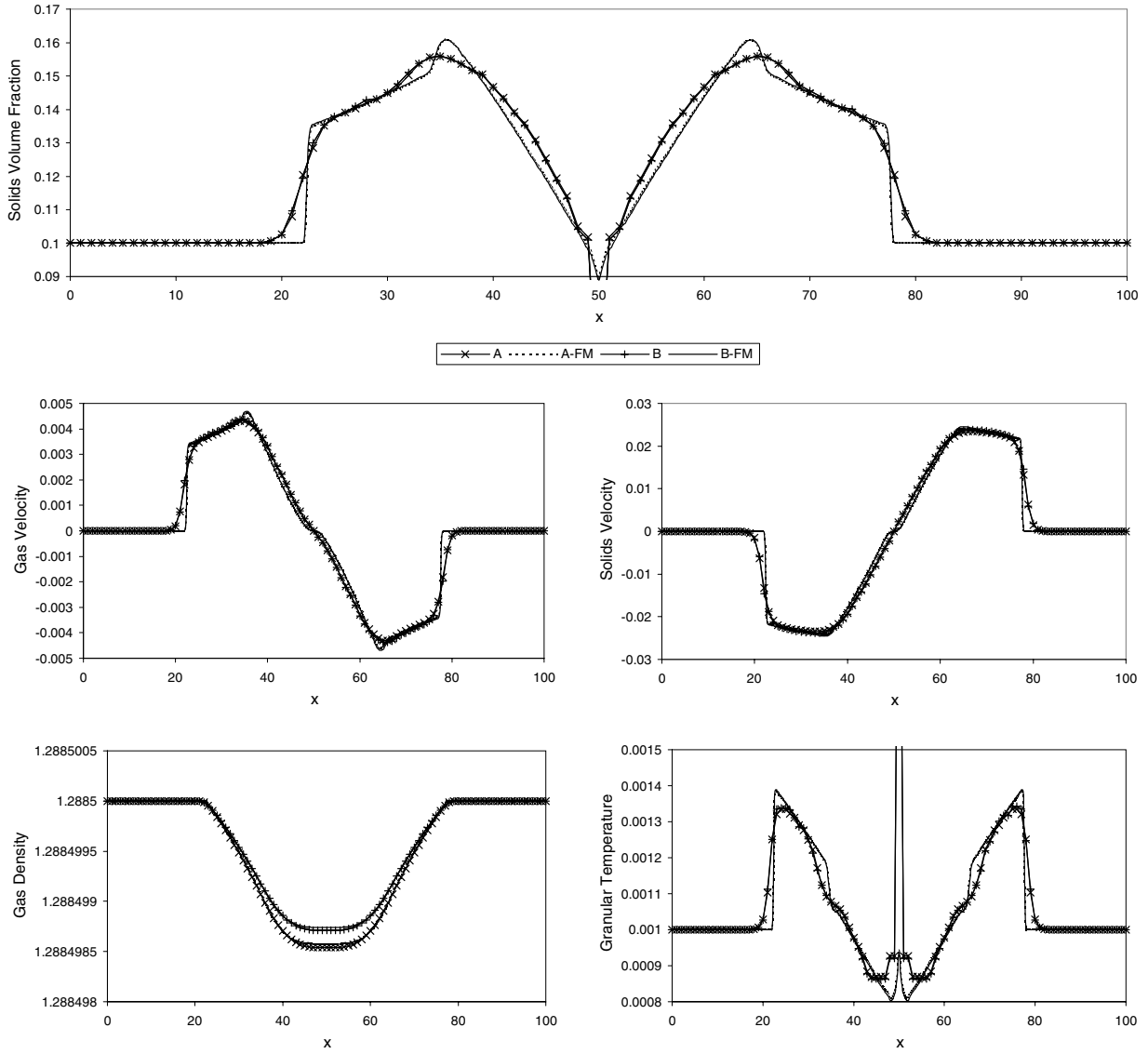

Fig. 7. Results for the square pulse test problem at $t = 200$ s (CP).

5.3. Steady state test problem

The simplest family of steady state solutions are obtained by setting the velocities equal, i.e., $u_g = u_s$. The inter-phase drag force is then zero. For our purposes, a better steady state solution of the model is one with different velocities so that the drag force is included.

For the general system, a steady state solution exists if the discharges for both phases are constant, i.e.,

$$Q_g = \epsilon_g \rho_g u_g \quad \text{and} \quad Q_s = \epsilon_s \rho_s u_s,$$

and the three ordinary differential equations

$$Q_g (u_g)_x + \omega_1 (p_g)_x + \omega_2 (p_s)_x = -\beta(u_g - u_s), \tag{10a}$$

$$Q_s (u_s)_x + \omega_3 (p_g)_x + \omega_4 (p_s)_x = \beta(u_g - u_s), \tag{10b}$$

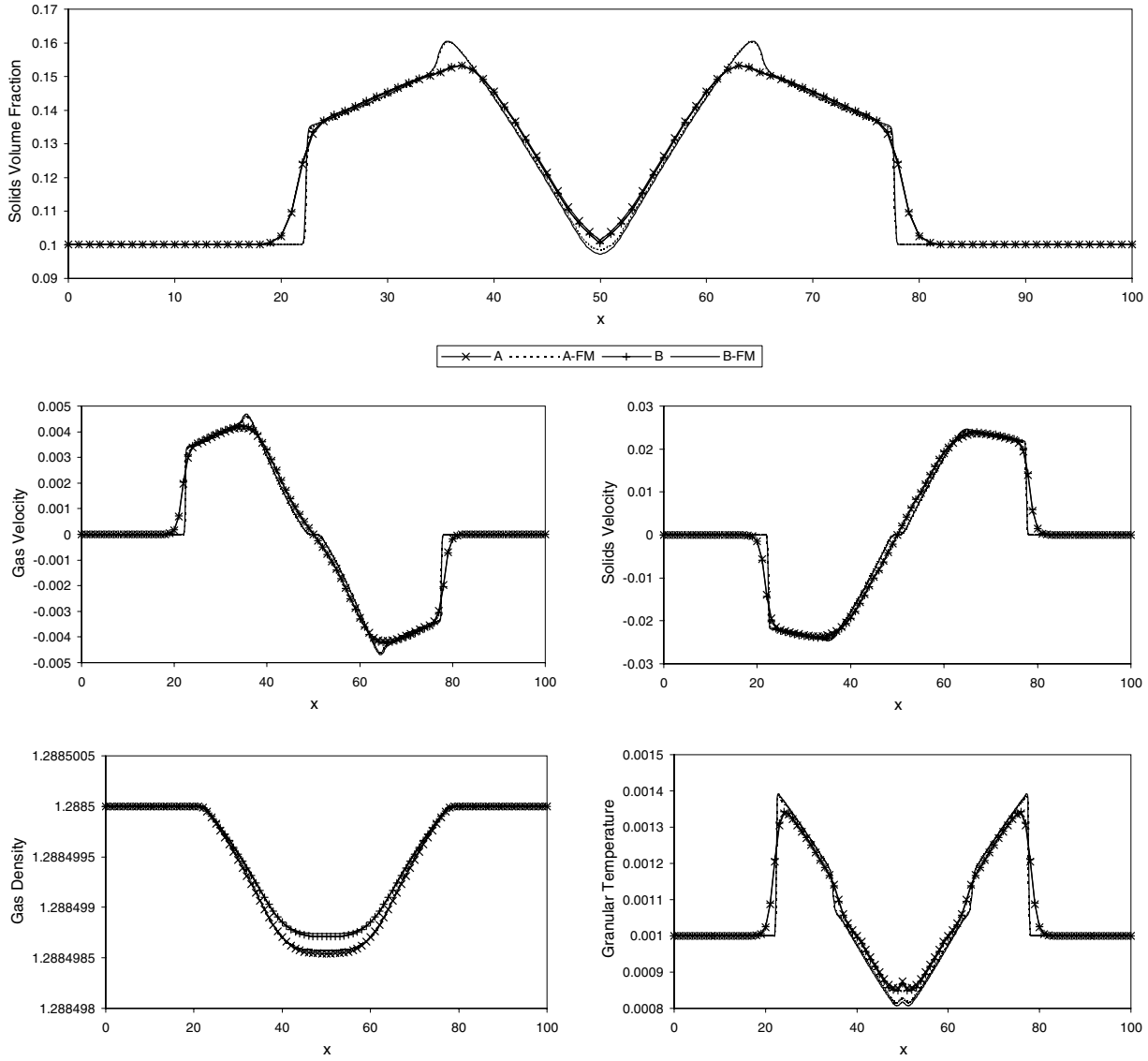

Fig. 8. Results for the square pulse test problem at $t = 200$ s (PW).

and

$$Q_s(T_s)_x = -\frac{2}{3}(p_s(u_s)_x + \gamma - (\kappa(T_s)_x)_x + 3\beta T_s) \tag{10c}$$

are satisfied.

To obtain a steady state solution for non-equal velocities, different velocities are imposed at the upstream boundary and the scheme iterated until a steady state has been reached. The initial conditions are:

$$\rho_g(x,0) = 1.2885, \quad u_g(x,0) = u_g^0,$$
$$\epsilon_s(x,0) = 0.1, \quad u_s(x,0) = 1 \quad \text{and} \quad T_s(x,0) = 0.1$$

with boundary conditions

$$\rho_g(100,t) = 1.2885, \quad u_g(0,t) = u_g^0, \tag{11a}$$
$$\epsilon_s(0,t) = 0.1, \quad u_s(0,t) = 1 \quad \text{and} \quad T_s(0,t) = 0.001. \tag{11b}$$

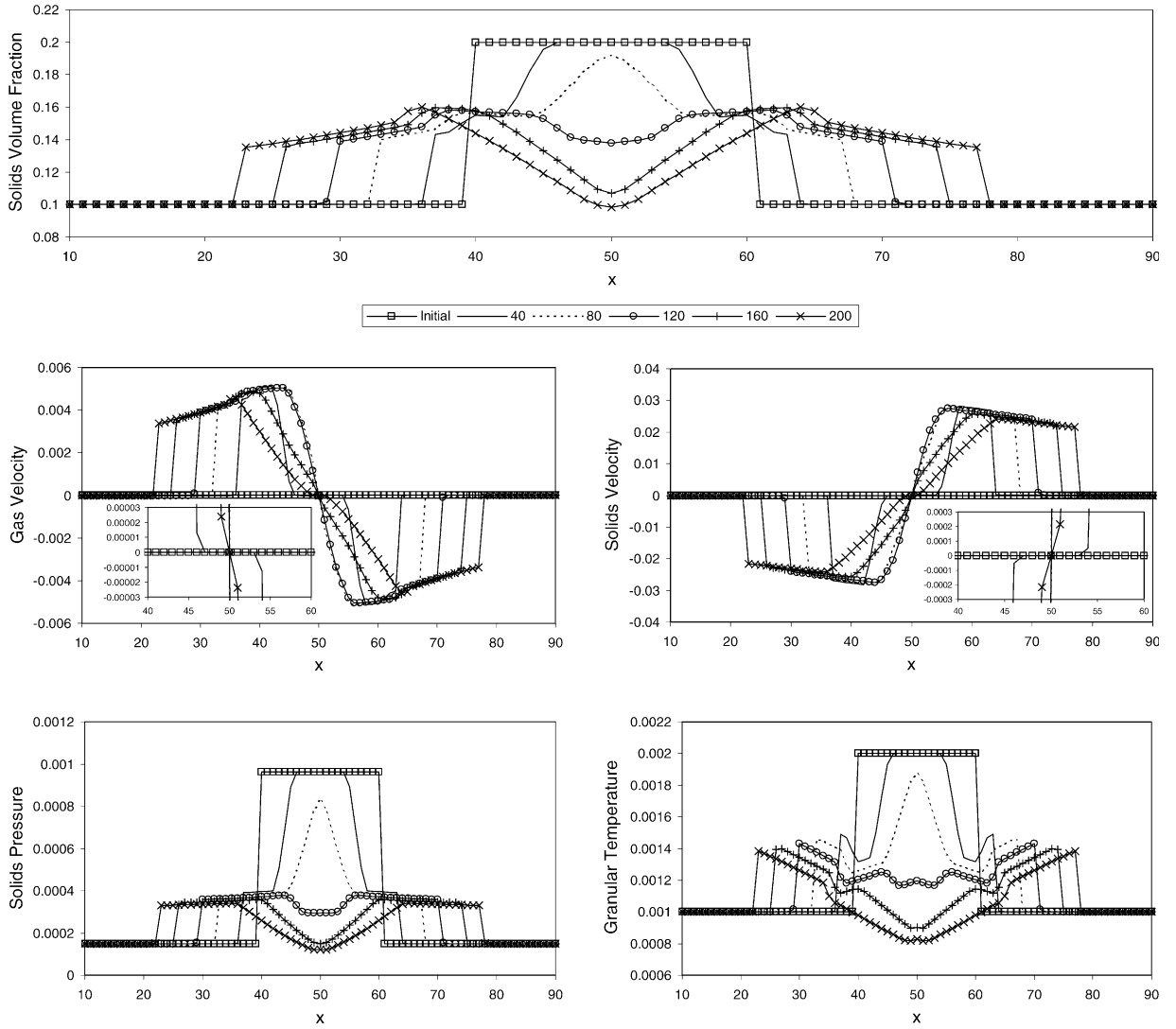

Fig. 9. Fine mesh results for the square pulse test problem for $t = 0$–200 s (PW).

The condition for a steady state to have been reached is

$$|\mathbf{w}_i^{n+1} - \mathbf{w}_i^n| \leqslant \text{tol} \quad \forall i,$$

where tol = 1E − 8.

Figs. 10 and 11 illustrate a comparison of the different models using either $u_g^0 = 1.5$ m/s or $u_g^0 = 5$ m/s, respectively. All models were approximated using the high resolution scheme with the van Leer flux-limiter (9) and the upwind approach for the inhomogeneous terms. Two spatial step sizes were used: the standard $\Delta x = 1$ m and a fine mesh (FM) of $\Delta x = 0.1$ m.

The results show that as the gas velocity is increased, the gradient of the variables at the upstream boundary increases due to the drag force dominating the pressure gradient terms as the difference between the velocities becomes larger. From Eqs. (10a) and (10b)

$$(u_g - u_s)_x + \left(\frac{\omega_1}{Q_g} - \frac{\omega_3}{Q_s}\right)(p_g)_x + \left(\frac{\omega_2}{Q_g} - \frac{\omega_4}{Q_s}\right)(p_s)_x = -\beta^0 \left(\frac{Q_g + Q_s}{Q_g Q_s}\right)(u_g - u_s)^2,$$

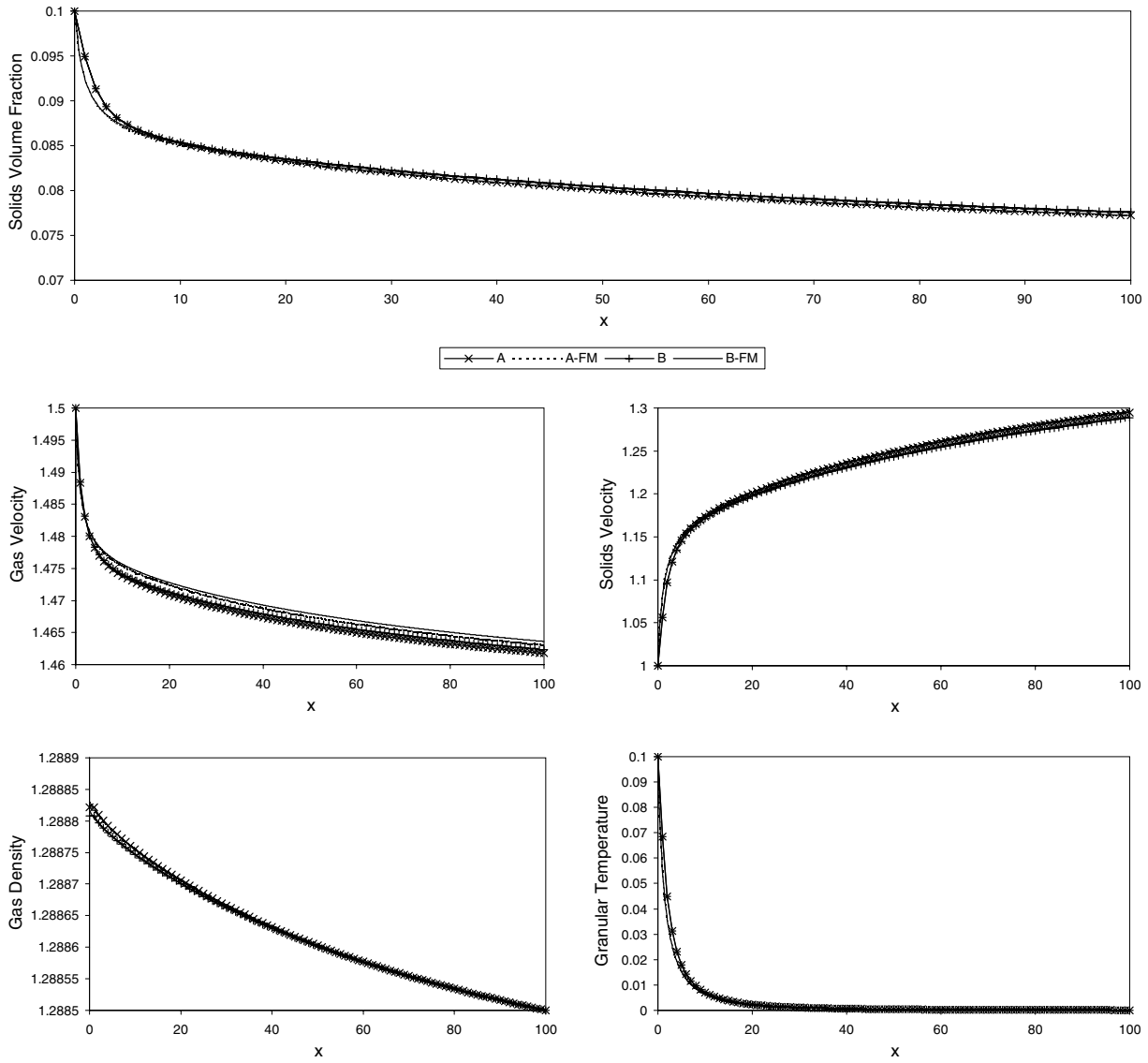

Fig. 10. Results for the steady state test problem with $u_g^0 = 1.5$ m/s.

where the drag force has been simplified and β^0 is assumed to be a constant

$$\beta^0 = \frac{3C_D}{4d_s}\rho_g^0\epsilon_g^0\epsilon_s^0$$

obtained from the boundary values (denoted by a ^{0} superscript). Supposing the drag force is large compared with the pressure gradient terms, the latter may be neglected and we obtain an equation for the difference in velocities

$$(u_g - u_s)_x = -\beta^0\left(\frac{Q_g + Q_s}{Q_g Q_s}\right)(u_g - u_s)^2$$

with solution

$$u_g - u_s = \frac{u_g^0 - u_s^0}{\beta^0\left(\frac{Q_g+Q_s}{Q_g Q_s}\right)(u_g^0 - u_s^0)x + 1}.$$

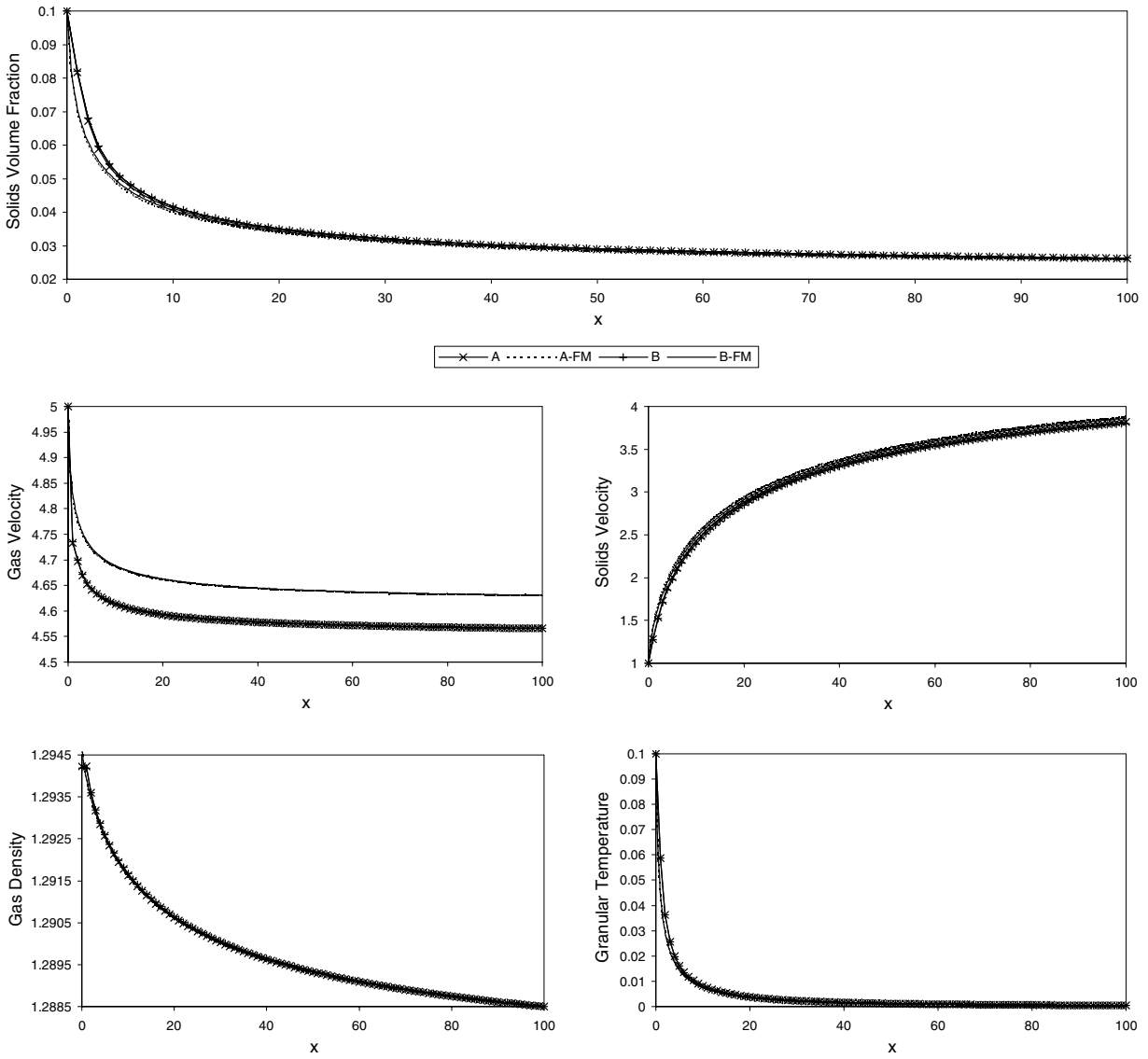

Fig. 11. Results for the steady state test problem with $u_g^0 = 5$ m/s.

Fig. 12 illustrates this equation for the boundary values (11) with $u_g^0 = 2$–5. Notice that there is a vertical asymptote close to the origin,

$$x^* = \frac{-1}{\beta^0 \left(\frac{Q_g + Q_s}{Q_g Q_s}\right)(u_g^0 - u_s^0)},$$

which gets closer to the origin as the difference between $u_g - u_s$ increases.

As the difference between the velocities increases at the upstream boundary, a kink becomes discernible a distance Δx, (one grid point) away from the upstream boundary and is due to the effect of the drag force on the gradient in the variables at the upstream boundary. As the difference between the two velocities increases, the gradient increases at the upstream boundary and the kink becomes more prominent. This may be rectified by using a finer space mesh so that the gradient is more accurately calculated. As the difference between the velocities increases, e.g. $u_g - u_s > 5$, the drag force term becomes "stiff" and the scheme becomes unstable.

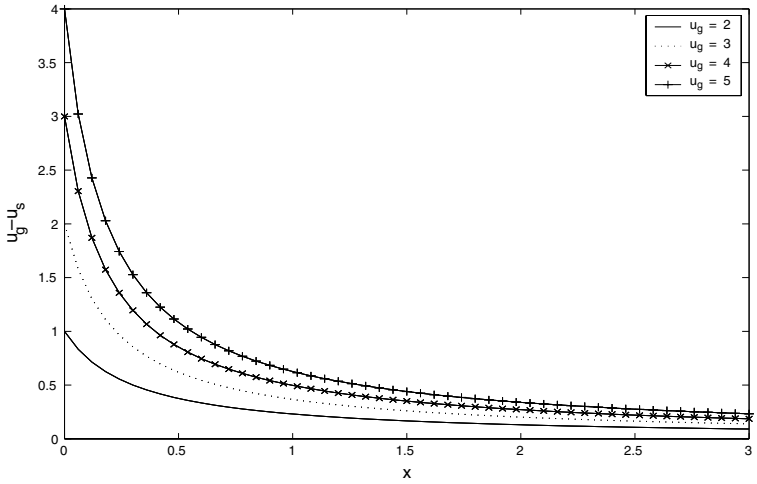

Fig. 12. Illustration of the significance of the drag force.

This test case is very sensitive to the type of flux-limiter. If the min mod limiter (8) is used then numerical oscillations are produced in the solids variables whereas the van Leer (9) limiter produces no numerical oscillations. If the Superbee limiter of Roe [33] is used, the numerical scheme becomes unstable. Model A is more sensitive to the type of limiter than Model B, which may be due to Model A being conditionally hyperbolic and the model contains more inhomogeneous terms than Model B. Model A remains hyperbolic for this test case, but the dissipation term (γ) in the fluctuating energy Eq. (3e) reduces the granular temperature towards zero. Using a larger value of T_s at the upstream boundary increases the gradient in the variables there. The numerical scheme also becomes unstable for $T_s \geqslant 1$. Using smaller values of T_s at the upstream boundary causes Model A to be hyperbolic only near the upstream boundary.

Concerning the inter-phase drag force, in Model B, if gravity is present Gidaspow [11] deduced that the drag force coefficient must be replaced with

$$\beta_B = \beta_A \epsilon_s^{-1}$$

in order for Archimedes principle to be satisfied. In the problems considered here, gravity is absent and so the same drag force coefficient was used in both models. Boemer et al. [4] also illustrated a difference between the models for certain test cases of 2D fluidized beds. They deduced that Model B results in a physical modification of the problem which can lead to an artificial increase in the forces carrying the particles. Moreover, even though Model A is deemed to be more physically correct than Model B, Boemer et al. also demonstrated that Model B produced numerical results that were closer to experiments than Model A.

6. Conclusion

In this paper, we have presented a general Eulerian two-phase gas–solid flow model and discussed three different variations of this model. We discretised the general system by using a high resolution scheme and investigated the different models for three different test cases.

The results for the different models are given above. The high resolution scheme needed to be slightly adapted (e.g. a different limiter or discretisation of the inhomogeneous terms) for certain test cases in order to ensure that no numerical oscillations or kinks developed. Other test cases were also investigated, which are not presented in this paper. When approximating the inhomogeneous terms with first order derivatives, the upwind method (7) is more accurate than the pointwise method (6) for test cases where the solids velocity was not close to zero. When the solids velocity was sufficiently close to zero, the pointwise method is superior to the upwind method, the latter producing numerical kinks in the results. Moreover, if the solids velocity changes sign, a numerical problem occurs at the stagnation point, which is not present with the pointwise method,

thereby illustrating that the problem is mainly due to the approximation of the inhomogeneous terms. This is in contrast to other systems of inhomogeneous conservation laws (e.g. shallow water equations, Euler equations, etc.), where the pointwise method has been known to produce inaccurate results. Sweby [40] also discovered a situation for the Euler equations where the pointwise method was superior to the upwind method.

The high resolution scheme is sensitive to the type of limiter used, some test cases requiring the van Leer limiter (9), others requiring the minmod limiter (8) to minimise numerical oscillations. The choice of limiter can affect the stability of the scheme when applied to inhomogeneous terms (see Hudson [18] and Hubbard and Garcia-Navarro [16]), the scheme was sensitive to the choice of limiter when the pointwise method is used for the inhomogeneous terms.

We have demonstrated that Model A is hyperbolic for a region of small relative velocities, due the inclusion of the solids pressure in the solids phase momentum equation. The size of the region is dependent on the values of ϵ_s, T_s and ρ_g. Model B is unconditionally well-posed whereas Model C is only well posed for $u_g = u_s$ or for large relative velocities. For small relative velocities, the regime of physical interest, Model A remains well-posed, although it becomes ill-posed as $T_s \to 0$.

For the test cases investigated here, the gas density ρ_g remains almost constant and the gradient of gas pressure is small. Models A and B only differ due to the gas pressure derivatives thus, there is little difference between them if the gradient of the gas pressure term is negligible.

A final conclusion is that both Models A and B can be accurately approximated using the high resolution scheme presented in this paper. Model A has the better physical foundation, so the fact that the presence of the solids pressure increases the regime of well-posedness, leads to the final conclusion that Model A is preferable for gas-grain two phase flow.

Acknowledgment

We would like to thank the Engineering and Physical Science Research Council for their funding under grant number GR/R85761/01.

Appendix A. Derivation of Roe average values

The numerical scheme discussed in Section 4.2 is based on Roe's scheme [32] and thus, requires Roe averaged values. In this section, we briefly outline the derivation of the Roe averaged values for the general system.

A.1. Roe averages

We first obtain a Roe averaged Jacobian matrix, $\tilde{\mathbf{A}}(\mathbf{w}_L, \mathbf{w}_R)$, which satisfies the following u-properties [32],

- $\tilde{\mathbf{A}}(\mathbf{w}_L, \mathbf{w}_R)$ must be diagonalisable with real eigenvalues (hyperbolicity);
- $\tilde{\mathbf{A}}(\mathbf{w}_L, \mathbf{w}_R) \to \tilde{\mathbf{A}}(\mathbf{w})$ as $\mathbf{w}_L, \mathbf{w}_R \to \mathbf{w}$ (consistency);
- $\Delta\mathbf{F} = \tilde{\mathbf{A}}(\mathbf{w}_L, \mathbf{w}_R)\Delta\mathbf{w}$ (conservation).

We obtain such a Roe averaged Jacobian by using the conservation u-property to obtain Roe averaged values of the variables. For our general system, we must satisfy

$$\Delta\mathbf{F} = \tilde{\mathbf{A}}\Delta\mathbf{w},$$

where

$$\tilde{\mathbf{A}} = \begin{bmatrix} 0 & 1 & 0 & 0 & 0 \\ \tilde{\epsilon}_g^{-1}\tilde{c}_g^2 - \tilde{u}_g^2 & 2\tilde{u}_g & \tilde{\rho}_g\tilde{\epsilon}_g^{-1}\tilde{c}_g^2 & 0 & 0 \\ 0 & 0 & 0 & 1 & 0 \\ 0 & 0 & \tilde{\epsilon}_s\tilde{T}_s\tilde{c_0}^2 - \tilde{u}_s^2 & 2\tilde{u}_s & \tilde{d}_0 \\ 0 & 0 & -\tilde{u}_s\tilde{T}_s & \tilde{T}_s & \tilde{u}_s \end{bmatrix}, \quad \mathbf{w} = \begin{bmatrix} \epsilon_g\rho_g \\ \epsilon_g\rho_g u_g \\ \epsilon_s \\ \epsilon_s u_s \\ \epsilon_s T_s \end{bmatrix} \quad \text{and} \quad \mathbf{F} = \begin{bmatrix} \epsilon_g\rho_g u_g \\ \epsilon_g\rho_g u_g^2 + p_g \\ \epsilon_s u_s \\ \epsilon_s u_s^2 + \epsilon_s T_s d_0 \\ \epsilon_s u_s T_s \end{bmatrix}.$$

Thus, we must ensure that:

$$\Delta(\epsilon_g\rho_g u_g) = \Delta(\epsilon_g\rho_g u_g), \tag{A.1a}$$
$$\Delta(\epsilon_g\rho_g u_g^2) + \Delta p_g = (\tilde{c}_g^2\tilde{\epsilon}_g^{-1} - \tilde{u}_g^2)\Delta(\epsilon_g\rho_g) + 2\tilde{u}_g\Delta(\epsilon_g\rho_g u_g) + \tilde{\rho}_g\tilde{\epsilon}_g^{-1}\tilde{c}_g^2\Delta\epsilon_s, \tag{A.1b}$$
$$\Delta(\epsilon_s u_s) = \Delta(\epsilon_s u_s), \tag{A.1c}$$
$$\Delta(\epsilon_s u_s^2) + \Delta(\epsilon_s T_s d_0) = (\tilde{\epsilon}_s\tilde{T}_s\tilde{c_0}^2 - \tilde{u}_s^2)\Delta\epsilon_s + 2\tilde{u}_s\Delta(\epsilon_s u_s) + \tilde{d}_0\Delta(\epsilon_s T_s), \tag{A.1d}$$
$$\Delta(\epsilon_s u_s T_s) = -\tilde{u}_s\tilde{T}_s\Delta\epsilon_s + \tilde{T}_s\Delta(\epsilon_s u_s) + \tilde{u}_s\Delta(\epsilon_s T_s). \tag{A.1e}$$

Clearly, Eqs. (A.1a) and (A.1c) are automatically satisfied. To obtain Roe average values of the velocities, we let:

$$\tilde{u}_g^2\Delta(\epsilon_g\rho_g) - 2\tilde{u}_g\Delta(\epsilon_g\rho_g u_g) + \Delta(\epsilon_g\rho_g u_g^2) = 0,$$
$$\tilde{u}_s^2\Delta\epsilon_s - 2\tilde{u}_s\Delta(\epsilon_s u_s) + \Delta(\epsilon_s u_s^2) = 0.$$

Thus, by obtaining the roots of these two quadratic equations (of $\tilde{u}_k$) we can use one of the roots for the Roe averaged value,

$$\tilde{u}_g = \frac{\sqrt{(\epsilon_g\rho_g)_L}(u_g)_L + \sqrt{(\epsilon_g\rho_g)_R}(u_g)_R}{\sqrt{(\epsilon_g\rho_g)_L} + \sqrt{(\epsilon_g\rho_g)_R}} \quad \text{and} \quad \tilde{u}_s = \frac{\sqrt{(\epsilon_s)_L}(u_s)_L + \sqrt{(\epsilon_s)_R}(u_s)_R}{\sqrt{(\epsilon_s)_L} + \sqrt{(\epsilon_s)_R}}.$$

We can now obtain

$$\tilde{T}_s = \frac{\sqrt{(\epsilon_s)_L}(T_s)_L + \sqrt{(\epsilon_s)_R}(T_s)_R}{\sqrt{(\epsilon_s)_L} + \sqrt{(\epsilon_s)_R}}$$

by substituting $\tilde{u}_s$ into (A.1e) and simplifying.

Thus, we only have two equations left to satisfy:

$$\tilde{\epsilon}_g\Delta p_g = \tilde{c}_g^2(\Delta(\epsilon_g\rho_g) - \tilde{\rho}_g\Delta\epsilon_g), \tag{A.2a}$$
$$\Delta(\epsilon_s T_s d_0) = \tilde{\epsilon}_s\tilde{T}_s\tilde{c_0}^2\Delta\epsilon_s + \tilde{d}_0\Delta(\epsilon_s T_s). \tag{A.2b}$$

We can simplify (A.2a) by letting

$$\tilde{c}_g^2 = \frac{\Delta p_g}{\Delta\rho_g}$$

and substituting into (A.2a), thus,

$$\Delta(\epsilon_g\rho_g) = \tilde{\epsilon}_g\Delta\rho_g + \tilde{\rho}_g\Delta\epsilon_g.$$

Here, we have two options:

$$\tilde{\epsilon}_k = \frac{1}{2}((\epsilon_k)_L + (\epsilon_k)_R) \quad \text{and} \quad \tilde{\rho}_g = \frac{1}{2}((\rho_g)_L + (\rho_g)_R) \tag{A.3}$$

or

$$\tilde{\epsilon}_k = \sqrt{(\epsilon_k)_L(\epsilon_k)_R} \quad \text{and} \quad \tilde{\rho}_g = \frac{\sqrt{(\epsilon_g)_L}(\rho_g)_L + \sqrt{(\epsilon_g)_R}(\rho_g)_R}{\sqrt{(\epsilon_g)_L} + \sqrt{(\epsilon_g)_R}}. \tag{A.4}$$

We can also satisfy (A.2b) by letting

$$\tilde{c}_0^2 = \frac{\Delta d_0}{\Delta\epsilon_s}$$

and substituting into (A.2b),

$$\Delta(\epsilon_s T_s d_0) = \tilde{\epsilon}_s \tilde{T}_s \Delta d_0 + \tilde{d}_0 \Delta(\epsilon_s T_s).$$

Hence,

$$\tilde{d}_0 = \frac{\Delta(\epsilon_s T_s d_0) - \tilde{\epsilon}_s \tilde{T}_s \Delta d_0}{\Delta(\epsilon_s T_s)}.$$

If the Roe averages (A.4) are used, then $\tilde{d}_0$ simplifies to

$$\tilde{d}_0 = \frac{\sqrt{(\epsilon_s)_L}(d_0)_L + \sqrt{(\epsilon_s)_R}(d_0)_R}{\sqrt{(\epsilon_s)_L} + \sqrt{(\epsilon_s)_R}}$$

Thus, all the Roe average values have been obtained. Notice that these values ensure that the other u-properties are satisfied.

A.2. Eigenvalues and eigenvectors

The eigenvalues and eigenvectors are obtained directly from the Roe averaged Jacobian matrix. We can easily obtain the eigenvalues

$$\tilde{\lambda}_{1,2} = \tilde{u}_g \mp \tilde{c}_g \sqrt{\tilde{\epsilon}_g^{-1}}, \quad \tilde{\lambda}_3 = \tilde{u}_s \quad \text{and} \quad \tilde{\lambda}_{4,5} = \tilde{u}_s \mp \sqrt{\tilde{T}_s(\tilde{d}_0 + \tilde{\epsilon}_s \tilde{c}_o^2)}.$$

The eigenvectors are determined in terms of the numerical eigenvalues and are obtained by solving

$$\begin{bmatrix} -\tilde{\lambda} & 1 & 0 & 0 & 0 \\ \tilde{\epsilon}_g^{-1}\tilde{c}_g^2 - \tilde{u}_g^2 & 2\tilde{u}_g - \tilde{\lambda} & \tilde{\rho}_g \tilde{\epsilon}_g^{-1} \tilde{c}_g^2 & 0 & 0 \\ 0 & 0 & -\tilde{\lambda} & 1 & 0 \\ 0 & 0 & \tilde{\epsilon}_s \tilde{T}_s \tilde{c_0}^2 - \tilde{u}_s^2 & 2\tilde{u}_s - \tilde{\lambda} & \tilde{d}_0 \\ 0 & 0 & -\tilde{u}_s \tilde{T}_s & \tilde{T}_s & \tilde{u}_s - \tilde{\lambda} \end{bmatrix} \begin{bmatrix} 1 \\ e_2 \\ e_3 \\ e_4 \\ e_5 \end{bmatrix} = 0.$$

Thus,

$$e_2 = \tilde{\lambda}, \tag{A.5a}$$

$$\tilde{\epsilon}_g^{-1}\tilde{c}_g^2 - \tilde{u}_g^2 + (2\tilde{u}_g - \tilde{\lambda})e_2 + \tilde{\rho}_g \tilde{\epsilon}_g^{-1} \tilde{c}_g^2 e_3 = 0, \tag{A.5b}$$

$$e_4 = \tilde{\lambda} e_3, \tag{A.5c}$$

$$(\tilde{\epsilon}_s \tilde{T}_s \tilde{c_0}^2 - \tilde{u}_s^2)e_3 + (2\tilde{u}_s - \tilde{\lambda})e_4 + \tilde{d}_0 e_5 = 0, \tag{A.5d}$$

$$-\tilde{u}_s \tilde{T}_s e_3 + \tilde{T}_s e_4 + (\tilde{u}_s - \tilde{\lambda})e_5 = 0. \tag{A.5e}$$

Now, by substituting (A.5a) into (A.5b), we obtain

$$e_3 = \frac{\tilde{u}_g^2 \tilde{\epsilon}_g - \tilde{c}_g^2 - (2\tilde{u}_g - \tilde{\lambda})\tilde{\epsilon}_g \tilde{\lambda}}{\tilde{\rho}_g \tilde{c}_g^2} = \frac{(\tilde{\lambda} - \tilde{u}_g)^2 \tilde{\epsilon}_g - \tilde{c}_g^2}{\tilde{\rho}_g \tilde{c}_g^2}.$$

Also, by substituting (A.5c) into (A.5d), we obtain

$$e_5 = \frac{e_3}{\tilde{d}_0}\left((\tilde{\lambda} - \tilde{u}_s)^2 - \tilde{\epsilon}_s \tilde{T}_s \tilde{c}_0^2\right).$$

Hence, we obtain

$$\tilde{\mathbf{e}}_{1,2} = \begin{bmatrix} 1 \\ \tilde{\lambda}_{1,2} \\ 0 \\ 0 \\ 0 \end{bmatrix} \quad \text{and} \quad \tilde{\mathbf{e}}_{3,4,5} = \begin{bmatrix} 1 \\ \tilde{\lambda}_{3,4,5} \\ \tilde{d}_{3,4,5} \\ \tilde{\lambda}_{3,4,5}\tilde{d}_{3,4,5} \\ \frac{\tilde{d}_{3,4,5}}{\tilde{d}_0}\left((\tilde{\lambda}_{3,4,5} - \tilde{u}_s)^2 - \tilde{\epsilon}_s\tilde{T}_s\tilde{c}_0^2\right) \end{bmatrix},$$

where

$$\tilde{d}_k = \frac{(\tilde{\lambda}_k - \tilde{u}_g)^2\tilde{\epsilon}_g - \tilde{c}_g^2}{\tilde{\rho}_g\tilde{c}_g^2}.$$

A.3. Wave strengths

We obtain wave strengths through the decomposition,

$$\Delta\mathbf{w} = \sum_{k=1}^{5} \tilde{\alpha}_k\tilde{\mathbf{e}}_k,$$

which for the general system results in solving

$$\Delta(\epsilon_g\rho_g) = \tilde{\alpha}_1 + \tilde{\alpha}_2 + \tilde{\alpha}_3 + \tilde{\alpha}_4 + \tilde{\alpha}_5, \tag{A.6a}$$

$$\Delta(\epsilon_g\rho_g u_g) = \tilde{\lambda}_1\tilde{\alpha}_1 + \tilde{\lambda}_2\tilde{\alpha}_2 + \tilde{\lambda}_3\tilde{\alpha}_3 + \tilde{\lambda}_4\tilde{\alpha}_4 + \tilde{\lambda}_5\tilde{\alpha}_5, \tag{A.6b}$$

$$\Delta\epsilon_s = \tilde{d}_3\tilde{\alpha}_3 + \tilde{d}_4\tilde{\alpha}_4 + \tilde{d}_5\tilde{\alpha}_5, \tag{A.6c}$$

$$\Delta(\epsilon_s u_s) = \tilde{\lambda}_3\tilde{d}_3\tilde{\alpha}_3 + \tilde{\lambda}_4\tilde{d}_4\tilde{\alpha}_4 + \tilde{\lambda}_5\tilde{d}_5\tilde{\alpha}_5, \tag{A.6d}$$

$$\tilde{d}_0\Delta(\epsilon_s T_s) = \tilde{d}_3\left((\tilde{\lambda}_3 - \tilde{u}_s)^2 - \tilde{\epsilon}_s\tilde{T}_s\tilde{c}_0^2\right)\tilde{\alpha}_3 + \tilde{d}_4\left((\tilde{\lambda}_4 - \tilde{u}_s)^2 - \tilde{\epsilon}_s\tilde{T}_s\tilde{c}_0^2\right)\tilde{\alpha}_4 + \tilde{d}_5\left((\tilde{\lambda}_5 - \tilde{u}_s)^2 - \tilde{\epsilon}_s\tilde{T}_s\tilde{c}_0^2\right)\tilde{\alpha}_5 \tag{A.6e}$$

for $\tilde{\alpha}_k$. The algebraic expressions obtained by solving this set of simultaneous equations $\tilde{\alpha}_{1,2}$ are complicated. To keep the algebraic expressions in a compact form, we solve (A.6c)–(A.6e) to obtain $\tilde{\alpha}_{3,4,5}$,

$$\tilde{\alpha}_k = \frac{(\tilde{\lambda}_a\tilde{\lambda}_b - \tilde{u}_s^2 + \tilde{\epsilon}_s\tilde{T}_s\tilde{c}_0^2)\Delta\epsilon_s - (\tilde{\lambda}_a + \tilde{\lambda}_b - 2\tilde{u}_s)\Delta(\epsilon_s u_s) + \tilde{d}_0\Delta(\epsilon_s T_s)}{\tilde{d}_k(\tilde{\lambda}_k - \tilde{\lambda}_a)(\tilde{\lambda}_k - \tilde{\lambda}_b)},$$

where $k \neq a \neq b$, and then solve $\tilde{\alpha}_{1,2}$ in terms of the other wave strengths,

$$\tilde{\alpha}_{1,2} = \mp\frac{\tilde{\lambda}_3\tilde{\alpha}_3 + \tilde{\lambda}_4\tilde{\alpha}_4 + \tilde{\lambda}_5\tilde{\alpha}_5 - (\tilde{\alpha}_3 + \tilde{\alpha}_4 + \tilde{\alpha}_5 - \Delta(\epsilon_g\rho_g))\tilde{\lambda}_{2,1} - \Delta(\epsilon_g\rho_g u_g)}{\tilde{\lambda}_1 - \tilde{\lambda}_2}.$$

Moreover, by substituting the expressions for $\tilde{\lambda}_k$ and using

$$\tilde{\epsilon}_s\tilde{T}_s\tilde{c}_0^2\Delta\epsilon_s + \tilde{d}_0\Delta(\epsilon_s T_s) = \Delta(\epsilon_s T_s d_0) \quad \text{and} \quad \Delta(\epsilon_s u_s) = \tilde{u}_s\Delta\epsilon_s + \tilde{\epsilon}_s\Delta u_s, \tag{A.7}$$

we obtain

$$\tilde{\alpha}_3 = -\frac{\tilde{d}_0\tilde{\epsilon}_s\Delta T_s}{\tilde{d}_3\tilde{c}_s^2} \quad \text{and} \quad \tilde{\alpha}_{4,5} = \frac{1}{2\tilde{d}_{4,5}\tilde{c}_s^2}(\Delta(\epsilon_s T_s d_0) \mp \tilde{c}_s\tilde{\epsilon}_s\Delta u_s),$$

where $\tilde{c}_s^2 = \tilde{T}_s(\tilde{d}_0 + \tilde{\epsilon}_s\tilde{c}_0^2)$.

A.4. Inhomogeneous terms

The values of $\tilde{\beta}_k$ are also determined from the decomposition,

$$\Delta x\tilde{\mathbf{R}} = \sum_{k=1}^{5} \tilde{\beta}_k \tilde{\mathbf{e}}_k,$$

which for the general system results in solving

$$0 = \tilde{\beta}_1 + \tilde{\beta}_2 + \tilde{\beta}_3 + \tilde{\beta}_4 + \tilde{\beta}_5, \tag{A.8a}$$

$$(1-\omega_1)\Delta p_g - \rho_s\omega_2\Delta(\epsilon_s T_s d_0) = \tilde{\lambda}_1\tilde{\beta}_1 + \tilde{\lambda}_2\tilde{\beta}_2 + \tilde{\lambda}_3\tilde{\beta}_3 + \tilde{\lambda}_4\tilde{\beta}_4 + \tilde{\lambda}_5\tilde{\beta}_5, \tag{A.8b}$$

$$0 = \tilde{d}_3\tilde{\beta}_3 + \tilde{d}_4\tilde{\beta}_4 + \tilde{d}_5\tilde{\beta}_5, \tag{A.8c}$$

$$-\frac{\omega_3}{\rho_s}\Delta p_g + (1-\omega_4)\Delta(\epsilon_s T_s d_0) = \tilde{\lambda}_3\tilde{d}_3\tilde{\beta}_3 + \tilde{\lambda}_4\tilde{d}_4\tilde{\beta}_4 + \tilde{\lambda}_5\tilde{d}_5\tilde{\beta}_5, \tag{A.8d}$$

$$-\frac{2}{3}\tilde{d}_0^2\tilde{\epsilon}_s\tilde{T}_s\Delta u_s = \tilde{d}_3\left((\tilde{\lambda}_3-\tilde{u}_s)^2 - \tilde{\epsilon}_s\tilde{T}_s\tilde{c}_0^2\right)\tilde{\beta}_3 + \tilde{d}_4\left((\tilde{\lambda}_4-\tilde{u}_s)^2 - \tilde{\epsilon}_s\tilde{T}_s\tilde{c}_0^2\right)\tilde{\beta}_4 + \tilde{d}_5\left((\tilde{\lambda}_5-\tilde{u}_s)^2 - \tilde{\epsilon}_s\tilde{T}_s\tilde{c}_0^2\right)\tilde{\beta}_5 \tag{A.8e}$$

for $\tilde{\beta}_k$. As with the wave strengths, algebraic expressions of $\tilde{\beta}_{1,2}$ are complicated. Thus, we solve (A.8c)–(A.8e) to obtain $\tilde{\beta}_{3,4,5}$,

$$\tilde{\beta}_k = \frac{(2\tilde{u}_s - \tilde{\lambda}_a - \tilde{\lambda}_b)\tilde{r}_4 + \tilde{d}_0\tilde{r}_5}{\tilde{d}_k(\tilde{\lambda}_k - \tilde{\lambda}_a)(\tilde{\lambda}_k - \tilde{\lambda}_b)},$$

where $k \neq a \neq b$, and then solve $\tilde{\beta}_{1,2}$ in terms of the other values of $\tilde{\beta}$,

$$\tilde{\beta}_{1,2} = \mp\frac{\tilde{\lambda}_3\tilde{\beta}_3 + \tilde{\lambda}_4\tilde{\beta}_4 + \tilde{\lambda}_5\tilde{\beta}_5 - (\tilde{\beta}_3 + \tilde{\beta}_4 + \tilde{\beta}_5)\tilde{\lambda}_{2,1} - \tilde{r}_2}{\tilde{\lambda}_1 - \tilde{\lambda}_2},$$

where

$$\tilde{r}_2 = (1-\omega_1)\Delta p_g - \rho_s\omega_2\Delta(\epsilon_s T_s d_0), \quad \tilde{r}_4 = -\frac{\omega_3}{\rho_s}\Delta p_g + (1-\omega_4)\Delta(\epsilon_s T_s d_0) \quad \text{and} \quad \tilde{r}_5 = -\frac{2}{3}\tilde{d}_0\tilde{\epsilon}_s\tilde{T}_s\Delta u_s.$$

Appendix B. *C*-property proof

To demonstrate that the numerical scheme satisfies the *C*-property, we apply the following basic steady state solution to the numerical scheme,

$$\rho_g = R, \quad u_g = u_s = 0, \quad \epsilon_s = G(x) \quad \text{and} \quad T_s = \frac{L}{\epsilon_s d_0}.$$

For this steady state solution, the discharges and pressures are constant and $r_s = 1$ with $\kappa = 0$. When the diffusion and dissipation terms of fluctuating energy are present, i.e., γ and κ, boundary conditions are required in order to obtain a steady state solution since these two terms imply that $T_s \to 0$. Similarly, the two velocities must be equal since, in the presence of the drag force, the two velocities tend to equality if no boundary conditions are prescribed. Thus, the above steady state solution is the only viable test case without applying boundary conditions.

When we apply this steady state solution to the numerical scheme, the eigenvalues become,

$$\tilde{\lambda}_{1,2} = \mp\tilde{c}_g\sqrt{\tilde{\epsilon}_g^{-1}}, \quad \tilde{\lambda}_3 = 0 \quad \text{and} \quad \tilde{\lambda}_{4,5} = \mp\tilde{c}_s,$$

with corresponding eigenvectors

$$\tilde{\mathbf{e}}_{1,2} = \begin{bmatrix} 1 \\ \tilde{\lambda}_{1,2} \\ 0 \\ 0 \\ 0 \end{bmatrix}, \quad \tilde{\mathbf{e}}_k^3 = \begin{bmatrix} 1 \\ 0 \\ \tilde{d}_3 \\ 0 \\ -\frac{\tilde{d}_3}{\tilde{d}_0}\tilde{\epsilon}_s\tilde{T}_s\tilde{c}_0^2 \end{bmatrix} \quad \text{and} \quad \tilde{\mathbf{e}}_k^{4,5} = \begin{bmatrix} 1 \\ \tilde{\lambda}_k \\ \tilde{d}_k \\ \tilde{\lambda}_k\tilde{d}_k \\ \tilde{d}_k\tilde{T}_s \end{bmatrix}.$$

Since the pressures are constant, the wave strengths simplify to

$$\tilde{\alpha}_{1,2} = \frac{1}{2}(\Delta(\epsilon_g \rho_g) - \tilde{\alpha}_3), \quad \tilde{\alpha}_3 = \frac{R\tilde{d}_0\tilde{\epsilon}_s \Delta T_s}{\tilde{c}_s^2} \quad \text{and} \quad \tilde{\alpha}_{4,5} = 0$$

and the inhomogeneous terms are all zero, i.e., $\tilde{\beta}_k = 0$.

We can simplify $\tilde{\alpha}_{1,2}$ even further to

$$\tilde{\alpha}_{1,2} = -\frac{R}{2\tilde{c}_s^2}\left(\tilde{c}_s^2 \Delta\epsilon_s + \tilde{d}_0\tilde{\epsilon}_s \Delta T_s\right) = -\frac{R}{2\tilde{c}_s^2}\left(\tilde{T}_s\tilde{d}_0 \Delta\epsilon_s + \tilde{T}_s\tilde{\epsilon}_s\tilde{c}_0^2 \Delta\epsilon_s + \tilde{d}_0\tilde{\epsilon}_s \Delta T_s\right)$$

and by using (A.7),

$$\tilde{\alpha}_{1,2} = -\frac{R}{2\tilde{c}_s^2}\left(\tilde{T}_s\tilde{\epsilon}_s\tilde{c}_0^2 \Delta\epsilon_s + \tilde{d}_0 \Delta(\epsilon_s T_s)\right) = -\frac{R}{2\tilde{c}_s^2}\Delta(\epsilon_s T_s d_0) = 0.$$

Thus, since $\tilde{\alpha}_k|\tilde{\lambda}_k| = 0$ for all k, the numerical flux-function becomes

$$\mathbf{F}^*_{i+\frac{1}{2}} = \begin{bmatrix} 0 \\ p_g \\ 0 \\ L \\ 0 \end{bmatrix} \Rightarrow \mathbf{F}^*_{i+\frac{1}{2}} - \mathbf{F}^*_{i-\frac{1}{2}} = 0.$$

Hence, the scheme is exact when applied to this steady state solution and, thus, satisfies the *C*-property.

Appendix C. The gas energy equation

For non-isentropic flow, the gas energy equation

$$(\epsilon_g E_g)_t + (u_g(\epsilon_g E_g + \omega_1 p_g + \omega_2 p_s))_x + p_g(\omega_1)_t + p_s(\omega_2)_t = -\beta u_g(u_g - u_s)$$

is appended to the model (3), where the total energy per unit volume is

$$E_g = \left(e_g + \frac{1}{2}u_g^2\right)\rho_g$$

and the specific internal energy (for ideal gases) is

$$e_g = \frac{p_g}{(\gamma_g - 1)\rho_g} \Rightarrow p_g = (\gamma_g - 1)\left(E_g - \frac{1}{2}\rho_g u_g^2\right).$$

For further discussion on the presence of the time derivatives $(\omega_k)_t$, see Gidaspow [13]. The analysis presented in this paper indicates that Model A remains conditionally hyperbolic and Model B unconditionally hyperbolic when the gas energy equation is included.

References

[1] M.R. Baer, J.W. Nunziato, A two-phase mixture theory for the deflagration-to-detonation transition in reactive granular materials, Int. J. Multiphase Flow 12 (6) (1986) 861–889.
[2] J.B. Bdzil, R. Meikoff, S.F. Son, A.K. Kapila, D.S. Stewart, Two-phase modeling of deflagration-to-detonation transition in granular materials: a critical examination of modelling issues, Phys. Fluid 11 (2) (1999) 378–402.
[3] A. Bermúdez, M.E. Vázquez, Upwind methods for hyperbolic conservation laws with source terms, Comp. Fluid 23 (8) (1994) 1049–1071.
[4] A. Boemer, H. Qi, U. Renz, Eulerian simulation of bubble formation at a jet in a two-dimensional fluidized bed, Int. J. Multiphase Flow 23 (5) (1997) 927–944.
[5] J.X. Bouillard, R.W. Lyczkowski, D. Gidaspow, Porosity distributions in a fluidized bed with an immersed obstacle, AIChE J. 35 (1989) 908–992.
[6] J. Ding, D. Gidaspow, A bubbling fluidization model using kinetic theory of granular flow, AIChE J. 36 (4) (1990) 523–538.
[7] D.A. Drew, Mathematical modelling of two-phase flow, Ann. Rev. Fluid Mech. 15 (1983) 261–291.

[8] B. Eindfelt, C.D. Munz, P.L. Roe, B. Sjogreen, On Godunov-type methods near low densities, J. Comput. Phys. 92 (1991) 273–292.
[9] M.R. Foster, P.W. Duck, R.E. Hewitt, The unsteady Karman problem for a dilute particle suspension, J. Fluid Mech. 474 (2003) 379–409.
[10] Li. Gascon, J.M. Corberan, Construction of second-order TVD schemes for nonhomogeneous hyperbolic conservation laws, J. Comput. Phys. 172 (2001) 261–297.
[11] D. Gidaspow, Hydrodynamics of fluidization and heat transfer: supercomputer modelling, Appl. Mech. Rev. 39 (1) (1986) 1–23.
[12] D. Gidaspow, R. Bezburuah, J. Ding, Hydrodynamics of circulating fluidized beds; kinetic theory approach, in: Fluidization VII, Proceedings of the 7th Engineering Foundation Conference on Fluidization, 1992, pp. 75–82.
[13] D. Gidaspow, Multiphase Flow and Fluidization, Academic Press, New York, 1994, ISBN 0122824709.
[14] D. Harris, E.F. Grekova, A hyperbolic well-posed model for the flow of granular materials, J. Eng. Math. 52 (2005) 107–135.
[15] A. Harten, High resolution schemes for conservation laws, J. Comput. Phys. 49 (1983) 357–393.
[16] M.E. Hubbard, P. Garcia-Navarro, Flux difference splitting and the balancing of source terms and flux gradients, J. Comput. Phys. 165 (2000) 89–125.
[17] N. Huber, M. Sommerfeld, Modelling and numeric calculation of dilute-phase pneumatic conveying in pipe systems, Powder Technol. 99 (1998) 90–101.
[18] J. Hudson, Numerical Techniques for Morphodynamic Modelling, Ph.D. Thesis, University of Reading, October 2001. A colour postscript version of this thesis can be obtained at <www.rdg.ac.uk/maths>.
[19] R. Jackson, The mechanics of fluidized beds. I: The stability of the state of uniform fluidization, Trans. Inst. Chem. Eng. 41 (1963) 13–21.
[20] R. Jackson, Locally averaged equations of motion for a mixture of identical spherical particles and a Newtonian fluid, Chem. Eng. Sci. 52 (1997) 2457–2469.
[21] R. Jackson, The Dynamics of Fluidized Particles, Cambridge Monographs on Mechanics, ISBN 0-521-78122-1, 2000.
[22] Kunal Jain, Deliang Shi, J.J. McCarthy, Discrete characterization of cohesion in gas–solid flows, Powder Technol. 146 (2004) 160–167.
[23] J.T. Jenkins, S.B. Savage, A theory for the rapid flow of identical, smooth, nearly elastic spherical particles, J. Fluid Mech. 130 (1983) 187–202.
[24] G.E. Klinzing, R.D. Marcus, F. Rizk, L.S. Leung, Pneumatic Conveying of Solids: A Theoretical and Practical Approach, Powder Technology Series, Chapman & Hall, London, 1997, ISBN 0 412 72440 5.
[25] R.J. LeVeque, Balancing source terms and flux gradients in high-resolution Godunov methods: the quasi-steady wave propagation algorithm, J. Comput. Phys. 146 (1998) 346–365.
[26] R.J. LeVeque, Finite Volume Methods for Hyperbolic Problems, Cambridge Tezts In Applied Mathematics, ISBN 0 521 00924 3, 2002.
[27] R.J. LeVeque, H.C. Yee, A study of numerical methods for hyperbolic conservation laws with stiff source terms, J. Comput. Phys. 86 (1990) 187–210.
[28] C.K.K. Lun, S.B. Savage, D.J. Jeffrey, N. Chepurnity, Kinetic theories for granular flow: inelastic particles in Couette flow and slightly inelastic particles in a general flowfield, J. Fluid Mech. 140 (1983) 223–256.
[29] R.W. Lyczkowski, Transient propagation behavior of two-phase flow equations, AIChE Symp. Ser. 75 (174) (1978) 165–174.
[30] R.W. Lyczkowski, D. Gidaspow, C.W. Solbrig, E.D. Hughes, Characteristics and stability analyses of transient one-dimensional two-phase flow equations and their finite difference approximations, Nucl. Sci. Eng. 66 (1978) 378–396.
[31] J.M. Powers, Two-phase flow viscous modeling of compaction of granular materials, Phys. Fluids 7 (1964) 1747–1754.
[32] P.L. Roe, Approximate Riemann solvers, parameter vectors and difference schemes, J. Comput. Phys. 43 (1981) 357–372.
[33] P.L. Roe, Some contributions to the modelling of discontinuous flows, Lect. Note Appl. Math. 22 (1985) 163–193.
[34] G. Rudinger, A. Chang, Analysis of non-steady two-phase flow, Phys. Fluid 7 (1964) 1747–1754.
[35] R.S. Saurel, R. Abgrall, A multiphase Godunov method for compressible multifluid and multiphase flows, J. Comput. Phys. 150 (1999) 425–467.
[36] R.S. Saurel, O. Lemetayer, A multiphase model for compressible flows with interfaces, shocks, detonation waves and cavitation, J. Comput. Phys. 150 (1999) 425–467.
[37] S.B. Savage, D.J. Jeffrey, The stress tensor in a granular flow at high shear stress, J. Fluid Mech. 110 (1981) 255.
[38] H.B. Stewart, B. Wendroff, Two-phase flows: models and methods, J. Comput. Phys. 56 (1984) 363–409.
[39] P.K. Sweby, High resolution schemes using flux limiters for hyperbolic conservation laws, SIAM J. Numer. Anal. 21 (1984) 995.
[40] P.K. Sweby, TVD Schemes for Inhomogeneous Conservation Laws, Department of Mathematics, University of Reading.
[41] M. Syamlal, W. Rogers, T.J. O'Brian, MFIX Documentation, Theory Guide, Technical Note DOE/METC-94/1004, 1993.
[42] B. van Leer, Towards the ultimate conservative difference scheme II. Monotonicity and conservation combined in a second order scheme, J. Comput. Phys. 14 (1974) 361–370.